

Excitation of spiral density waves by convection in accretion discs

G. R. Mamatsashvili^{1,2,3*} and W. K. M. Rice¹

¹ SUPA, Institute for Astronomy, University of Edinburgh, Blackford Hill, Edinburgh EH9 3HJ, Scotland

² Abastumani Astrophysical Observatory, Iliia State University, 2a Kazbegi Ave., Tbilisi 0160, Georgia

³ Faculty of Exact and Natural Sciences, Tbilisi State University, 1 Chavchavadze Ave., Tbilisi 0128, Georgia

Accepted 2011 June 21. Received 2011 June 21; in original form 2011 January 31

ABSTRACT

Motivated by the recent results of Lesur & Ogilvie (2010) on the transport properties of incompressible convection in protoplanetary discs, in this paper we study the role of compressibility and hence of another basic mode – spiral density waves – in convective instability in discs. We analyse the linear dynamics of non-axisymmetric convection and spiral density waves in a Keplerian disc with superadiabatic vertical stratification using the local shearing box approach. It is demonstrated that the shear associated with Keplerian differential rotation introduces a novel phenomenon, it causes these two perturbation modes to become coupled: during evolution the convective mode generates (trailing) spiral density waves and can therefore be regarded as a new source of spiral density waves in discs. The wave generation process studied here owes its existence solely to shear of the disc’s differential rotation, and is a special manifestation of a more general linear mode coupling phenomena universally taking place in flows with an inhomogeneous velocity profile. We quantify the efficiency of spiral density wave generation by convection as a function of azimuthal and vertical wavenumbers of these modes and find that it is maximal and most powerful when both these length-scales are comparable to the disc scale height. We also show that unlike the convective mode, which tends to transport angular momentum inwards in the linear regime, the spiral density waves transport angular momentum outwards. Based on these findings, we suggest that in the non-linear regime spiral density waves generated by convection may play a role in enhancing the transport of angular momentum due the convective mode alone, which is actually being changed to outward by non-linearity, as indicated by above-mentioned recent developments.

Key words: accretion, accretion discs – hydrodynamics – instabilities – convection – (stars:)planetary systems: protoplanetary discs – turbulence

1 INTRODUCTION

The main agent responsible for the anomalous outward transport of angular momentum in protoplanetary accretion discs is widely recognised to be turbulence due to magnetorotational instability (MRI, Balbus & Hawley 1998; Balbus 2003). However, in order for the MRI to operate, the disc must be sufficiently ionised so that the gas and magnetic field are effectively coupled (Blaes & Balbus 1994; Sano et al. 2000; Sano & Stone 2002; Salmeron & Wardle 2003; Desch 2004). In cold and dense interiors of protoplanetary discs, the necessary level of ionisation is not typically reached and, as a result, a large magnetically inac-

tive region – ‘dead zone’ – develops in the disc (see e.g., Gammie 1996; Stone et al. 2000; Fromang et al. 2002). Several mechanisms have been put forward to explain (non-magnetic) transport in the dead zone: penetration/diffusion of turbulent fluctuations into the dead zone due to the MRI in the surface layers (Fleming & Stone 2003; Turner et al. 2007; Oishi et al. 2007; Oishi & Mac Low 2009), transport due to self-gravity (Armitage et al. 2001) and due to various hydrodynamic candidates, such as vortices, spiral density waves, Rossby wave and baroclinic instabilities (e.g., Lovelace et al. 1999; Li et al. 2001; Klahr & Bodenheimer 2003; Johnson & Gammie 2005b; Petersen et al. 2007; Johnson & Gammie 2006; Lesur & Papaloizou 2010).

Recent developments indicate that yet another mechanism – thermal convection in the vertical direction – can also

* E-mail: grm@roe.ac.uk

provide outward transport of angular momentum. Vertical convection was first suggested as a source of angular momentum transport in protoplanetary discs long before the MRI (Cameron 1978; Lin & Papaloizou 1980, 1985; Ruden & Lin 1986; Ruden & Pollack 1991). In these earlier studies, it was pointed out that the temperature dependence of the opacity in protoplanetary discs can lead to convective instability for a wide range of disc temperatures (see also Rafikov 2007). A corresponding effective viscosity was estimated based on a phenomenological mixing-length prescription and using this, evolutionary models of discs – with outward angular momentum transport driven solely by convective turbulence – were constructed. Ruden et al. (1988) carried out a linear analysis of axisymmetric convective modes in discs and, although linear axisymmetric modes do not produce torques themselves to transport angular momentum, these authors also estimated – from the radial wavelengths and growth rates of the most unstable axisymmetric modes – a Shakura-Sunyaev $\alpha \sim 10^{-3} - 10^{-2}$, which might be in the case of non-linear axisymmetric or non-axisymmetric vertical convection. However, the non-linear development of these axisymmetric (two-dimensional) convective modes turned out to lead to inward (i.e., towards the central star) transport of angular momentum (Kley et al. 1993; Rüdiger et al. 2002), which is obviously not what is required for the accretion of matter from the disc onto the central star.

To investigate the problem of convective transport more fully, subsequent studies considered the dynamics of non-axisymmetric convection in discs with Keplerian differential rotation, or shear. In this case, shear-induced effects (see below) come into play for non-axisymmetric perturbations and hence their dynamics is richer than that of axisymmetric ones. The linear studies of Korycansky (1992) and Ryu & Goodman (1992, hereafter RG92) in the shearing box framework showed that growing non-axisymmetric shearing waves of the convective mode in the trailing phase lead predominantly to inward transport of angular momentum. However, Lin et al. (1993) argued that this can be changed if the radial stratification, which is absent in the shearing box, is taken into account. A stratified background can support radially localised packets of the convective mode, which are able to provide an outward flux of angular momentum. Following more general non-linear three-dimensional simulations of convection by Cabot & Pollack (1992); Cabot (1996) and Stone & Balbus (1996), however, did not yield outward angular momentum transport either; the time-averaged α -parameter turned out to be small and negative, implying inward transport. This led to vertical convection being regarded as an inefficient mechanism for driving angular momentum transport and disc’s secular evolution. However, Klahr et al. (1999), using global disc simulations, demonstrated that convective flow can in fact be non-axisymmetric (i.e., have azimuthal structure) and pointed out that the small azimuthal extent of the computational domains and low Reynolds numbers in the simulations of Cabot (1996) and Stone & Balbus (1996) had a tendency to wipe out all azimuthal variations resulting in the near axisymmetry of convection, which as noted above, is characterised by inward transport of angular momentum.

Since high-resolution simulations with improved numerical techniques are becoming increasingly affordable, interest in convective transport is reviving. Lesur & Ogilvie (2010)

performed incompressible simulations of convective instability in the shearing box and found, contrary to previous results, that at high enough Rayleigh (Reynolds) numbers ($\gtrsim 10^6$), the sign of the corresponding α is reversed to positive, though it still remains small. This was demonstrated to be a consequence of the non-axisymmetric structure of convection, which is established at large Rayleigh numbers. This plays a central role in that it gives rise to an appreciable pressure-strain correlation tensor that, in turn, changes the direction of transport from inwards to outwards. Past simulations mentioned above, being at low Rayleigh (Reynolds) numbers, had thus been unable to capture the non-axisymmetry of convective flow. Analogous simulations by Käpylä et al. (2010) also showed that due to non-axisymmetry, convection can transport angular momentum outwards. However, the specific parameter range considered by these authors is somewhat different to that of Lesur & Ogilvie (2010). Although the findings of both these studies seem encouraging, they should be viewed as tentative and requiring further corroboration.

All the above-mentioned studies consider perturbation dynamics in a sheared environment, as the Keplerian differential rotation of protoplanetary discs is characterised by a strong radial shear of the azimuthal velocity. It is well known from fluid dynamical studies that operators governing the linear dynamics of perturbations in flows with non-uniform kinematics are non-normal due to the shear of the mean velocity profile, resulting in a number of linear transient, or finite-time phenomena (see e.g., Trefethen et al. 1993; Schmid & Henningson 2001, for an introduction to the subject). The standard modal approach (i.e., spectral expansion of perturbations in time and examination of eigenfrequencies), commonly employed in hydrodynamics (Drazin & Reid 1981), describes perturbation behaviour (stability) only at asymptotically large times; in fact it is unable to capture the transient dynamics of perturbations at intermediate times. In other words, predictions of the modal analysis concerning flow stability are really relevant only to the asymptotic fate of a flow. Accordingly, new mathematical methods – broadly known as the non-modal approach – had been developed that allow for the non-normality-induced perturbation dynamics (e.g., Schmid & Henningson 2001). The non-modal approach leads to an initial value problem, enabling us to trace a full temporal evolution of perturbations and in that respect it is advantageous over the modal approach.

One of the most important transient phenomenon, which is a consequence of the non-normality, is the coupling and energy exchange among different perturbation modes with each other and with the mean flow occurring during a finite time interval in the linear theory. The linear mode coupling is a general phenomenon intrinsic to inhomogeneous/shear flows (Chagelishvili et al. 1997) and plays an important role in the subsequent non-linear development of perturbations and largely defines the characteristics of the resulting non-linear state (turbulence). Because of strong Keplerian shear, similar non-normality/shear-induced transient processes should inevitably take place in discs as well. So, for a proper understanding of energy exchange processes in the non-linear regime and ultimately of disc turbulence phenomenon, it is necessary to first analyse in the linear regime all possible couplings and energy exchange channels

among perturbation modes existing in disc flows. As pointed out above, the modal approach, which has been as widely employed in studying perturbation dynamics in discs (e.g., Narayan et al. 1987; Lin et al. 1990; Lubow & Ogilvie 1998; Ogilvie & Lubow 1999; Li et al. 2003) as in fluid mechanics, does not account for a finite-time aspect of perturbation dynamics originating from the shear of disc flow. For this reason, when analysing temporal evolution of perturbations in discs, a different technique, a special type of the non-modal approach – the method of shearing waves – is often employed (e.g., RG92; Goldreich & Lynden-Bell 1965; Bodo et al. 2005; Johnson & Gammie 2005a; Heinemann & Papaloizou 2009a, hereafter HP09a), which we also adopt in this paper.

A special manifestation of the shear-induced linear mode coupling phenomena in discs is the generation of spiral density and inertia-gravity waves by vortices, which has already been extensively studied taking into account the presence of other factors specific to discs: radial and vertical stratifications, self-gravity, MRI turbulence, etc (Davis et al. 2000; Davis 2002; Tevzadze et al. 2003; Bodo et al. 2005; Johnson & Gammie 2005a,b; Bodo et al. 2007; Mamatsashvili & Chagelishvili 2007; Tevzadze et al. 2008; Mamatsashvili & Rice 2009; Heinemann & Papaloizou 2009a,b; Tevzadze et al. 2010). In particular, it was shown that an efficient generation of spiral density waves (SDWs) by vortices occurs when the characteristic horizontal length-scale of these two perturbation types is of the order of the disc thickness, which, in turn, implies that compressibility effects are important at such length-scales. The role SDWs play in disc dynamics cannot be overestimated. In particular, it was suggested that gravitational forces due to stochastic density perturbations associated with SDWs in a turbulent disc flow, may be important in the migration of low-mass planets (Nelson & Papaloizou 2004; Nelson 2005). More significantly, SDWs are able to enhance angular momentum transport rate (see e.g., Johnson & Gammie 2005b; Oishi & Mac Low 2009). SDWs also play a role in the dynamics and angular momentum transport in a dead zone (Fleming & Stone 2003; Oishi et al. 2007; Oishi & Mac Low 2009). So, it is crucial to identify and analyse the generation mechanisms of SDWs.

Our goal in this paper is to investigate yet another manifestation of shear-induced linear mode coupling phenomena in discs – generation of SDWs by convection. In a disc with superadiabatic vertical stratification, together with the convective mode due to a negative entropy gradient, there also exists a SDW mode due to compressibility. As we will show, Keplerian shear of the disc’s differential rotation causes the coupling of these two modes in a way similar to that of coupling of SDWs to vortices mentioned above. Since normally SDWs contribute to the angular momentum transport process, this coupling can in turn have important implications for convective transport as well. So, convection, like vortices, can be regarded as a new source of SDWs. However, we omit the vortical mode in this paper, because in the linear theory presented here, an exponentially growing convective mode is more powerful and dominates the algebraic growth of the vortical mode (unless the disc is self-gravitating). Following RG92, we treat a stratified disc in the local shearing box approximation. We examine in detail how the generation of the SDW mode by the convective mode occurs during evolution and quantify its efficiency as a function

of azimuthal and vertical wavelengths of these modes. We demonstrate that the efficiency of wave excitation is maximal and powerful when both these wavelengths are comparable to the disc scale height, that is, for wavelengths at which compressibility is important. Indeed, the above-mentioned numerical simulations indicate that convective motions (rolls) actually extend over the entire scale height of the disc and are characterised by moderate Mach numbers (see e.g., Stone & Balbus 1996), implying that compressibility and, hence SDWs, also actively participate in dynamical processes in convectively unstable discs and their effects must be understood properly. Finally, we would like to note that SDW generation can also be seen in the linear analysis of RG92 and also in a related linear study of the growth of non-axisymmetric shearing waves of the convective mode by Brandenburg & Dintrans (2006), though these authors do not specifically focus on and characterise this phenomenon.

The paper is organised as follows. Physical model and basic equations are introduced in Section 2. Shear-induced linear coupling of SDWs and convection is investigated in detail in Section 3. Angular momentum transport by these two modes is analysed in Section 4. Summary and discussion are presented in Section 5.

2 PHYSICAL MODEL AND EQUATIONS

To study the dynamics of perturbation modes existing in compressible and stratified gaseous discs with Keplerian rotation, we adopt a local shearing box approach of Goldreich & Lynden-Bell (1965). In the shearing box model, disc dynamics is studied in a local Cartesian reference frame co-rotating with the disc’s angular velocity at some fiducial radius r_0 from the central star, so curvature effects due to cylindrical geometry of the disc are ignored. In this coordinate frame, the unperturbed differential rotation of the disc manifests itself as a parallel azimuthal flow with a linear velocity shear in the radial direction. The Coriolis force is included to take into account the effects of the coordinate frame rotation. The vertical component of the gravity force of the central star is also present, but self-gravity of the disc is neglected. As a result, we can write down the three-dimensional shearing box equations of motion

$$\frac{d\mathbf{u}}{dt} + 2\Omega\hat{\mathbf{z}} \times \mathbf{u} + \nabla \left(-q\Omega^2 x^2 + \frac{1}{2}\Omega^2 z^2 \right) + \frac{1}{\rho}\nabla p = 0 \quad (1)$$

and continuity

$$\frac{d\rho}{dt} + \rho\nabla \cdot \mathbf{u} = 0. \quad (2)$$

Here $\mathbf{u} = (u_x, u_y, u_z)$ is the velocity of gas in the local frame; ρ and p are, respectively, the gas density and pressure; Ω is the angular velocity of the local rotating reference frame, which is equal to the disc’s angular velocity at r_0 : $\Omega(r_0)$; x, y, z are, respectively, the radial, azimuthal and vertical coordinates; $\hat{\mathbf{z}}$ is the unit vector along the vertical direction; $d/dt = \partial/\partial t + (\mathbf{u} \cdot \nabla)$ is the total time derivative operator. The shear parameter $q = 1.5$ for the Keplerian differential rotation considered in this paper.

In the absence of heat exchange, the specific entropy $s = c_v \ln(p/\rho^\gamma)$ of fluid elements is conserved along streamlines

$$\frac{ds}{dt} = 0, \quad (3)$$

where the adiabatic index $\gamma = c_p/c_v$ is the ratio of specific heats c_p and c_v at constant pressure and constant volume, respectively (for convenience, below we replace $s/c_v \rightarrow s$). It follows from equations (1-3) that Ertel's theorem of potential vorticity conservation holds

$$\frac{d}{dt} \frac{(\nabla \times \mathbf{u} + 2\Omega \hat{\mathbf{z}}) \cdot \nabla s}{\rho} = 0, \quad (4)$$

which we will make use of later in classifying perturbation modes in the disc.

2.1 The equilibrium disc model

Equations (1-3) have an equilibrium solution that is stationary and axisymmetric. In this unperturbed state, the velocity field of Keplerian rotation represents, as noted above, a parallel azimuthal flow, \mathbf{u}_0 , with a constant radial shear $-q\Omega$:

$$u_{x0} = u_{z0} = 0, \quad u_{y0} = -q\Omega x.$$

In the shearing box model, equilibrium density, ρ_0 , and pressure, p_0 , depend only on the vertical z -coordinate and satisfy the hydrostatic relation

$$g_0 \equiv -\frac{1}{\rho_0} \frac{dp_0}{dz} = \Omega^2 z. \quad (5)$$

Following RG92 and Brandenburg & Dintrans (2006), we assume the unperturbed disc to be vertically isothermal with a constant adiabatic sound speed

$$c_s = \sqrt{\gamma \frac{p_0}{\rho_0}}. \quad (6)$$

For simplicity, we use the thin disc approximation with constant gravity (see e.g., Shu 1974; Tevzadze et al. 2003, RG92). In other words, the vertically varying gravitational acceleration $\Omega^2 z$ is replaced with its some height-averaged constant value $g > 0$, but because the former has opposite signs on either side of the disc midplane $z = 0$, we write

$$g_0 = \Omega^2 z \rightarrow \text{sign}(z)g. \quad (7)$$

Although this simplification is highly idealised, it greatly facilitates the mathematical treatment of the problem allowing us to make Fourier analysis of perturbations in the vertical direction too in addition to horizontal decomposition into shearing waves (see below). This, in turn, makes it possible to clearly understand the key effects of shear on the dynamics of perturbation modes with various vertical and horizontal length-scales in a stratified disc and avoids the need to solve complex partial differential equations with respect to time t and the vertical coordinate z . In this case of constant g , substituting replacement (7) into equation (5) and using expression (6) for the vertically constant sound speed, we find the distribution of the equilibrium density and pressure with z :

$$\frac{\rho_0(z)}{\rho_m} = \frac{p_0(z)}{p_m} = \exp\left(-\frac{|z|}{H}\right), \quad (8)$$

where

$$H = \frac{c_s^2}{\gamma g}$$

is the vertical stratification scale height of the disc, $\rho_m \equiv \rho_0(0)$ and $p_m \equiv p_0(0)$ are the midplane values of the equilibrium density and pressure. As mentioned above, g is some height-averaged value of acceleration and we choose g^2 to be equal to the density-weighted average of $(\Omega^2 z)^2$, where as a weight function we use an exact expression for the equilibrium density, $\rho_m \exp(-\gamma \Omega^2 z^2 / 2c_s^2)$, which is obtained from equations (5) and (6) with a linearly increasing gravitational acceleration $\Omega^2 z$ (RG92). This relates to the angular velocity through

$$\Omega^2 = \frac{\gamma g^2}{c_s^2}.$$

The Brunt-Väisälä frequency squared is defined as

$$N_0^2 \equiv \frac{g_0}{\rho_0} \left(\frac{1}{c_s^2} \frac{dp_0}{dz} - \frac{d\rho_0}{dz} \right) = \frac{\gamma - 1}{\gamma} \Omega^2.$$

If $\gamma > 1$, then $N_0^2 > 0$ (subadiabatic thermal stratification) and the equilibrium vertical structure of the disc is convectively stable. For $\gamma < 1$, then $N_0^2 < 0$ (superadiabatic thermal stratification) corresponding to a convectively unstable equilibrium. For $\gamma = 1$ (adiabatic thermal stratification), $N_0^2 = 0$ and all motions/modes due to buoyancy disappear. Since our goal here is to investigate the linear coupling between vertical convection and SDWs and the possible role of this phenomenon in the disc dynamics and angular momentum transport, we focus, as in RG92, only on the superadiabatic vertical structure choosing $\gamma = 0.8$ throughout this paper. This value of γ is close to unity reflecting the fact that the degree of superadiabaticity is not very large in protoplanetary discs (Rafikov 2007). Strictly speaking, the case $\gamma < 1$ does not make much thermodynamic sense, because it implies $c_v > c_p$. In spite of this, there is no problem with equation (3) describing entropy conservation. In principle, the convectively unstable regime can be modelled without using the condition $\gamma < 1$, if we appropriately choose cooling and heating functions in the entropy equation (see also RG92). So, a simple γ -prescription mimics the basic features of convectively stable/unstable discs well without introducing additional heating and cooling functions that might unnecessarily complicate the situation.

2.2 Perturbation equations

Consider now small perturbations to the equilibrium state (8) with the background flow \mathbf{u}_0 . Linearising equations (1-3) about this state, we obtain the following system governing the perturbation dynamics

$$\frac{Du'_x}{Dt} = -\frac{1}{\rho_0} \frac{\partial p'}{\partial x} + 2\Omega u'_y, \quad (9)$$

$$\frac{Du'_y}{Dt} = -\frac{1}{\rho_0} \frac{\partial p'}{\partial y} + (q - 2)\Omega u'_x, \quad (10)$$

$$\frac{Du'_z}{Dt} = -\frac{1}{\rho_0} \frac{\partial p'}{\partial z} - g_0 \frac{\rho'}{\rho_0}, \quad (11)$$

$$\frac{D\rho'}{Dt} + \nabla \cdot (\rho_0 \mathbf{u}') = 0, \quad (12)$$

$$\frac{Ds'}{Dt} + \frac{\gamma N_0^2}{g_0} u'_z = 0, \quad (13)$$

where

$$\frac{D}{Dt} \equiv \frac{\partial}{\partial t} - q\Omega x \frac{\partial}{\partial y}$$

and \mathbf{u}' , ρ' , p' , s' are the perturbed velocity relative to the background Keplerian shear flow, perturbed density, pressure and entropy, respectively. From the definition of specific entropy above we also have the relation

$$s' = \frac{p'}{p_0} - \gamma \frac{\rho'}{\rho_0}. \quad (14)$$

The form of equations (9-13) permits a decomposition of the perturbed quantities into shearing plane waves, or spatial Fourier harmonics (SFH) with time-dependent amplitudes and phases,

$$\begin{pmatrix} u'_x(\mathbf{r}, t) \\ u'_y(\mathbf{r}, t) \\ u'_z(\mathbf{r}, t) \\ s'(\mathbf{r}, t) \end{pmatrix} = \begin{pmatrix} \hat{u}_x(t) \\ \hat{u}_y(t) \\ \hat{u}_z(t) \\ \hat{s}(t) \end{pmatrix} \exp\left(\frac{|z|}{2H}\right) \exp(ik_x(t)x + ik_y y + ik_z z), \quad (15)$$

$$\begin{pmatrix} \rho'(\mathbf{r}, t) \\ p'(\mathbf{r}, t) \end{pmatrix} = \begin{pmatrix} \hat{\rho}(t) \\ \hat{p}(t) \end{pmatrix} \exp\left(-\frac{|z|}{2H}\right) \exp(ik_x(t)x + ik_y y + ik_z z), \quad (16)$$

$$k_x(t) = q\Omega k_y t.$$

The azimuthal k_y and vertical k_z wavenumbers remain unchanged, whereas the radial wavenumber $k_x(t)$ varies with time at a constant rate $q\Omega k_y$ if $k_y \neq 0$ (i.e., for non-axisymmetric perturbations) due to sweeping of wave crests by the background shear flow. For convenience, in $k_x(t)$ we have shifted the origin of time towards negative values, so that for $t = 0$, $k_x(0) = 0$ as well. In this case, an initially leading SFH with $k_x(t)/k_y < 0$ at $t < 0$ eventually becomes trailing with $k_x(t)/k_y > 0$ at $t > 0$. This change of SFH's orientation from leading to trailing is called 'swing' and occurs when $k_x(t) = 0$. This technique of decomposition of perturbations into shearing waves was originally devised by Lord Kelvin (Thompson 1887) in order to study transiently growing solutions in inviscid incompressible parallel flows with linear shear. It is widely used today in various applications involving flows with a linear shear of velocity profile and greatly helps to grasp intermediate-time linear phenomena – transient growth and coupling of perturbation modes – in shear flows, which tend to be overlooked in the standard modal analysis. Besides, such shearing waves are really the only spectral basis compatible with shearing-periodic boundary conditions, which are almost always used in local simulations of accretion discs (see e.g., Hawley et al. 1995). We would also like to mention that recently it has been mathematically proven by Yoshida (2005) that shearing waves in fact represent the simplest/basic 'elements' of dynamical processes at linear shear. The exponential factors in (15) and (16) involving $\pm|z|/2H$ are necessary in order to compensate for otherwise exponentially increasing with height perturbation energy due to stratified equilibrium. With the latter form, the perturbation energy, proportional to $\rho_0 u'^2$, is vertically uniform when averaged over the vertical wavelength (see also Lerche & Parker 1967, RG92). The inclusion of these exponential factors also ensure that there are no imaginary terms in the dispersion relation de-

rived below that could lead us to infer some sort of spurious instability.

Substituting (15) and (16) into equations (9-14) and using replacement (7), we arrive at the following system of first order ordinary differential equations that govern the linear dynamics of SFHs of perturbations

$$\frac{d\hat{u}_x}{dt} = -ik_x(t) \frac{\hat{p}}{\rho_m} + 2\Omega \hat{u}_y, \quad (17)$$

$$\frac{d\hat{u}_y}{dt} = -ik_y \frac{\hat{p}}{\rho_m} + (q-2)\Omega \hat{u}_x, \quad (18)$$

$$\frac{d\hat{u}_z}{dt} = -\left(ik_z - \frac{\text{sign}(z)}{2H}\right) \frac{\hat{p}}{\rho_m} - \text{sign}(z)g \frac{\hat{\rho}}{\rho_m}, \quad (19)$$

$$\frac{d\hat{\rho}}{dt} = -\rho_m \left[ik_x(t)\hat{u}_x + ik_y \hat{u}_y + \left(ik_z - \frac{\text{sign}(z)}{2H}\right) \hat{u}_z \right], \quad (20)$$

$$\frac{d\hat{s}}{dt} = -\text{sign}(z) \frac{\gamma N_0^2}{g} \hat{u}_z, \quad (21)$$

$$\hat{s} = \frac{\hat{p}}{p_m} - \gamma \frac{\hat{\rho}}{\rho_m}. \quad (22)$$

Note that by means of the exponential factors in (15) and (16), we have rendered the coefficients in these equations z -independent, though they still contain the sign of z . Below we will reduce this set so that sign-dependence will disappear too.

It can be readily shown that the system (17-21) possesses an important time invariant – the linearised potential vorticity perturbation

$$I \equiv ik_x(t)\hat{u}_y - ik_y \hat{u}_x - (2-q)\Omega \left[\frac{\hat{p}}{\rho_m} - \frac{\text{sign}(z)g}{\gamma N_0^2} \left(ik_z - \frac{\text{sign}(z)}{2H} \right) \hat{s} \right] = \text{const},$$

whose conservation is a direct consequence of Ertel's potential vorticity theorem (4). This time invariant I , in turn, indicates the existence of the vortical/aperiodic mode in the perturbation spectrum, which is characterised by non-zero potential vorticity ($I \neq 0$) and represents a stationary (i.e., time-independent) solution of equations (17-21) in the absence of shear. In the present three-dimensional case, this vortical mode originates from the combined action of the vertical gravity force (stratification) and the Coriolis force and represents a 3D generalisation of the 2D vortical mode considered in Bodo et al. (2005); Johnson & Gammie (2005a); Mamatsashvili & Chagelishvili (2007); HP09a. Because of the shear/non-normality of disc flow, the vortical mode can undergo large transient amplification and effectively (linearly) couple with and excite other modes (SDWs, inertia-gravity waves, baroclinic modes, etc.) existing in the disc (Tevzadze et al. 2003; Bodo et al. 2005; Mamatsashvili & Chagelishvili 2007; Tevzadze et al. 2008, 2010, HP09a). However, in the linear regime considered here with no disc self-gravity, the transient (algebraic) growth of the vortical mode is overwhelmed by the exponential amplification of the convective mode, so we exclude the former mode from our analysis by setting the linearised potential vorticity to zero, $I = 0$. In the non-linear regime, however, the exponential growth of the convective mode is saturated,

so convection no longer dominates over vortices and both can equally take part in the SDW generation process.

Taking into account that by our choice $I = 0$, we can eliminate \hat{u}_x , \hat{u}_y , \hat{u}_z and \hat{p} in favour of $\hat{\rho}$ and \hat{s} in equations (17-22). Then, for convenience, switching to a new auxiliary quantity

$$\hat{l} = \frac{1}{k_{\perp}(t)} \left[\frac{1}{\gamma} + \frac{\text{sign}(z)g}{\gamma N_0^2} \left(ik_z - \frac{\text{sign}(z)}{2H} \right) \right]^{-1} \times \left[\frac{\hat{\rho}}{\rho_m} - \frac{\text{sign}(z)g}{\gamma N_0^2} \left(ik_z - \frac{\text{sign}(z)}{2H} \right) \hat{s} \right]$$

instead of the density $\hat{\rho}$, we finally arrive at the second order system with real coefficients forming the basis for our subsequent analysis,

$$\frac{d^2 \hat{l}}{dt^2} = -[c_s^2 k_{\perp}^2(t) + \kappa^2(t)] \hat{l} - c_s^2 k_{\perp}(t) \hat{s}, \quad (23)$$

$$\frac{d^2 \hat{s}}{dt^2} = k_{\perp}(t) \left[N_0^2 - c_s^2 \left(k_z^2 + \frac{1}{4H^2} \right) \right] \hat{l} - c_s^2 \left(k_z^2 + \frac{1}{4H^2} \right) \hat{s}, \quad (24)$$

where

$$\kappa^2(t) \equiv 2(2-q)\Omega^2 - \frac{4q\Omega^2 k_y^2}{k_{\perp}^2(t)} + \frac{3q^2\Omega^2 k_y^4}{k_{\perp}^4(t)}$$

and $k_{\perp}^2(t) = k_x^2(t) + k_y^2 = k_y^2(1 + q^2\Omega^2 t^2)$. Although the physical meaning of \hat{l} is less transparent, by taking its advantage we have reduced the original system (17-22) to a more compact one (23) and (24), with all the coefficients being real, in order to ease further manipulations and to make our equations friendlier for numerical treatment. Equations (23) and (24) contain all the information on various perturbation modes (apart from the vortical mode) present in a vertically stratified Keplerian disc. In the next section, we remove shear from these equations for the moment in order to classify modes in the disc and then put shear back again to see how it alters the mode dynamics and what new effects it introduces.

2.3 Classification of modes in the absence of shear

Consider first a simple case without shear (i.e., a rigidly rotating disc) by setting $q = 0$ in equations (23) and (24). After that, all the coefficients in these equations become time-independent and, therefore, we can look for solutions in the form $\hat{l}, \hat{s} \propto \exp(i\omega t)$. Substituting this into equations (23) and (24), we obtain the following dispersion relation in the absence of shear

$$\omega^4 - \left[c_s^2 k_{\perp}^2 + c_s^2 \left(k_z^2 + \frac{1}{4H^2} \right) + \kappa^2 \right] \omega^2 + c_s^2 \left[N_0^2 k_{\perp}^2 + \kappa^2 \left(k_z^2 + \frac{1}{4H^2} \right) \right] = 0,$$

where $\kappa^2 = 4\Omega^2$ is constant when $q = 0$. This dispersion relation has two different solutions corresponding to two different types of perturbation modes:¹

1. A high-frequency SDW mode with

$$\omega_s^2 = \frac{c_s^2 k_{\perp}^2 + c_s^2 (k_z^2 + 1/4H^2) + \kappa^2}{2} \times \left(1 + \sqrt{1 - \frac{4c_s^2 [N_0^2 k_{\perp}^2 + \kappa^2 (k_z^2 + 1/4H^2)]}{[c_s^2 k_{\perp}^2 + c_s^2 (k_z^2 + 1/4H^2) + \kappa^2]^2}} \right) \quad (25)$$

the restoring force for which is mainly provided by compressibility/pressure forces, but is modified by stratification/bouyancy and the Coriolis force. So, in this mode, pressure perturbations dominate over entropy perturbations. For large wavenumbers $k_{\perp}H, k_zH \gg 1$ (i.e., for wavelengths much smaller than the disc scale height), the effects of stratification and rotation are negligible and the frequency of the SDW mode reduces to $\omega_s^2 \simeq c_s^2(k_{\perp}^2 + k_z^2)$. In an unstratified disc, for z -independent perturbations (i.e., in the razor-thin disc approximation), from (25) we obtain $\omega_s^2 = c_s^2(k_x^2 + k_y^2) + \kappa^2$, which is a classical dispersion relation of two-dimensional SDWs in non-self-gravitating discs (see e.g., Balbus 2003) and therefore expression (25) can be regarded as a generalised form of the SDW mode frequency in the presence of vertical stratification.

2. A low-frequency inertia-bouyancy mode with

$$\omega_s^2 = \frac{c_s^2 k_{\perp}^2 + c_s^2 (k_z^2 + 1/4H^2) + \kappa^2}{2} \times \left(1 - \sqrt{1 - \frac{4c_s^2 [N_0^2 k_{\perp}^2 + \kappa^2 (k_z^2 + 1/4H^2)]}{[c_s^2 k_{\perp}^2 + c_s^2 (k_z^2 + 1/4H^2) + \kappa^2]^2}} \right) \quad (26)$$

the restoring force for which is mainly provided by vertical bouyancy and the Coriolis force, but modified by compressibility. So, in this mode, entropy perturbations dominate over pressure perturbations. The inertia-bouyancy mode represents an inertia-gravity wave in the case of subadiabatic and adiabatic stratifications ($N_0^2 \geq 0$) and the convective mode in the case of superadiabatic stratification ($N_0^2 < 0$), which is considered here.² The dynamics of inertia-gravity waves in Keplerian discs is extensively studied elsewhere (see e.g., Lubow & Pringle 1993; Ogilvie 1998; Balbus 2003; Tevzadze et al. 2003, 2008; Latter & Balbus 2009) and will not be dealt with here. Again, in the limit of large wavenumbers $k_{\perp}H, k_zH \gg 1$, the effect of compressibility on the inertia-bouyancy mode is small and we get the well-known dispersion relation $\omega_g^2 \simeq \frac{N_0^2 k_{\perp}^2 + \kappa^2 k_z^2}{k_{\perp}^2 + k_z^2}$, which can also be derived using the incompressible (Boussinesq) approximation (Tevzadze et al. 2008).

Thus, in a stratified compressible disc, perturbations can be classified into two basic types – the SDW and inertia-bouyancy modes (apart from the vortical mode) and any general perturbation (with zero potential vorticity) can be decomposed into the sum of these two modes. We should note, however, that the mode classification performed here is actually applicable in the case of the constant- g approximation (7), which is, strictly speaking, valid when characteristic

¹ If we included the vortical mode, it would correspond, as noted above, to the stationary solution $\omega = 0$, since $I \neq 0$ for this mode.

² Although we call this a convective mode, it actually exhibits convective instability (i.e., it has $\omega_g^2 < 0$) only when the wavenumbers satisfy $\kappa^2(k_z^2 + 1/4H^2) < -N_0^2 k_{\perp}^2$ in order to overcome the stabilising effect of rotation.

vertical length-scales of perturbations are less than the disc scale height. A more general classification of vertical modes in stratified discs without invoking this approximation is performed in Ruden et al. (1988); Lubow & Pringle (1993); Korycansky & Pringle (1995); Ogilvie (1998) (in these papers, the compressible p-mode corresponds to our SDW mode and the r- and convective g-modes to the inertia-buoyancy mode). Nevertheless, the classification adopted here allows us to grasp the key effects of shear on the dynamics of the inertia-buoyancy (convective) and SDW modes.

To analyse the behaviour of these two modes, we define new characteristic quantities, or eigenfunctions, ψ_s and ψ_g , for them as

$$\psi_s = \frac{k_\perp [c_s^2(k_z^2 + 1/4H^2) - N_0^2] \hat{l} - [\omega_g^2 - c_s^2(k_z^2 + 1/4H^2)] \hat{s}}{\omega_s^2 - \omega_g^2}, \quad (27)$$

$$\psi_g = \frac{k_\perp [c_s^2(k_z^2 + 1/4H^2) - N_0^2] \hat{l} - [\omega_s^2 - c_s^2(k_z^2 + 1/4H^2)] \hat{s}}{\omega_g^2 - \omega_s^2} \quad (28)$$

describing, respectively, the SDW and inertia-buoyancy modes. These eigenfunctions are convenient and physically revealing, as substituting them into equations (23) and (24) with shear terms removed, we obtain two separate equations for each mode eigenfunction

$$\frac{d^2 \psi_s}{dt^2} + \omega_s^2 \psi_s = 0, \quad \frac{d^2 \psi_g}{dt^2} + \omega_g^2 \psi_g = 0 \quad (29)$$

that allow us to study these modes individually. All the other quantities ($\hat{u}_x, \hat{u}_y, \hat{u}_z, \hat{\rho}, \hat{p}$) can be expressed through the mode eigenfunctions ψ_s, ψ_g and their respective first order time-derivatives. Hence, we can fully determine the perturbation field corresponding to a specific mode by setting the eigenfunction of the other mode and its time derivative to zero. In other words, if we want to have either only SDWs or the inertia-buoyancy mode in the disc flow, we should initially set simply $\psi_g(-\infty) = d\psi_g/dt(-\infty) = 0$ or $\psi_s(-\infty) = d\psi_s/dt(-\infty) = 0$, respectively. Modal equations (29) governing the dynamics of the SDW and inertia-buoyancy modes are not coupled, implying that in the absence of shear the perturbation modes evolve independently, that is, initially exciting one either mode with a specific characteristic time-scale does not lead to the excitation of other modes with different time-scales. In the following sections, we investigate how shear modifies modal equations (29) and its influence on the dynamics of the SDW and inertia-buoyancy modes. Specifically, we will show that in the presence of Keplerian shear, these equations are no longer independent from each other, i.e., become coupled that, in turn, results in the linear coupling between these two modes and, in particular, between SDWs and convection.

2.4 Effects of shear on mode dynamics

Here we derive the generalised modal equations from equations (23) and (24) including shear q . For the sake of further analysis, let us first non-dimensionalise the basic quantities by obvious units: time (frequencies) by means of the angular speed Ω ,

$$\Omega t \rightarrow t, \quad \frac{\omega_{s,g}}{\Omega} \rightarrow \omega_{s,g}, \quad \frac{\kappa^2}{\Omega^2} \rightarrow \kappa^2, \quad \frac{N_0^2}{\Omega^2} \rightarrow N_0^2 = \frac{\gamma - 1}{\gamma},$$

and length-scales (wavenumbers) as well as \hat{l} using c_s/Ω as a unit of length,

$$(K_x, K_y, K_z) = \frac{c_s}{\Omega}(k_x, k_y, k_z), \quad \frac{\Omega H}{c_s} \rightarrow H = \frac{1}{\sqrt{\gamma}}, \quad \frac{\Omega \hat{l}}{c_s} \rightarrow \hat{l}$$

(\hat{s}, ψ_s, ψ_g are already non-dimensional). Accordingly, the normalised radial wavenumber K_x varies with normalised time as $K_x(t) = qK_y t$. Also, as defined above, $K_\perp^2(t) = K_x^2(t) + K_y^2 = K_y^2(1 + q^2 t^2)$. Since $K_x(t)$ and $\kappa^2(t)$ in equations (25) and (26) are now time-dependent as a result of shear, the non-dimensional frequencies ω_s and ω_g also become functions of time:

$$\omega_s^2(t) = \frac{\kappa^2(t) + K_\perp^2(t) + K_z^2 + \gamma/4}{2} \times \left(1 + \sqrt{1 - \frac{4[N_0^2 K_\perp^2(t) + \kappa^2(t)(K_z^2 + \gamma/4)]}{[\kappa^2(t) + K_\perp^2(t) + K_z^2 + \gamma/4]^2}} \right)$$

$$\omega_g^2(t) = \frac{\kappa^2(t) + K_\perp^2(t) + K_z^2 + \gamma/4}{2} \times \left(1 - \sqrt{1 - \frac{4[N_0^2 K_\perp^2(t) + \kappa^2(t)(K_z^2 + \gamma/4)]}{[\kappa^2(t) + K_\perp^2(t) + K_z^2 + \gamma/4]^2}} \right).$$

At large times, $K_\perp(t) \rightarrow \infty$ and from these expressions it follows that $\omega_s^2(t) \simeq K_\perp^2(t)$, $\omega_g^2(t) \simeq N_0^2$. As noted above, all the other quantities can readily be expressed through ψ_s, ψ_g and their first order time derivatives, so we carry out the further analysis working mostly with the eigenfunctions.

Expressing \hat{l}, \hat{s} through ψ_s, ψ_g from equations (27) and (28) and substituting them into equations (23) and (24), we arrive at the following system of coupled second order differential equations for the eigenfunctions

$$\frac{d^2 \psi_s}{dt^2} + f_s \frac{d\psi_s}{dt} + (\omega_s^2 + \Delta\omega_s^2) \psi_s = f_g \frac{d\psi_g}{dt} + \Delta\omega_g^2 \psi_g, \quad (30)$$

$$\frac{d^2 \psi_g}{dt^2} + f_g \frac{d\psi_g}{dt} + (\omega_g^2 + \Delta\omega_g^2) \psi_g = f_s \frac{d\psi_s}{dt} + \Delta\omega_s^2 \psi_s, \quad (31)$$

where the new coefficients $f_s, \Delta\omega_s^2$ and $f_g, \Delta\omega_g^2$, compared with equations (29), describe modifications to the dynamics of the SDW and inertia-buoyancy modes and their coupling brought about by the shear of disc flow. They depend on time as well as on the azimuthal K_y and vertical K_z wavenumbers:

$$f_s(K_y, K_z, t) \equiv \frac{2K_\perp(t)}{\omega_s^2(t) - \omega_g^2(t)} \left(\frac{\omega_s^2(t) - K_z^2 - \gamma/4}{K_\perp(t)} \right)',$$

$$f_g(K_y, K_z, t) \equiv \frac{2K_\perp(t)}{\omega_g^2(t) - \omega_s^2(t)} \left(\frac{\omega_g^2(t) - K_z^2 - \gamma/4}{K_\perp(t)} \right)',$$

$$\Delta\omega_s^2(K_y, K_z, t) \equiv \frac{K_\perp(t)}{\omega_s^2(t) - \omega_g^2(t)} \left(\frac{\omega_s^2(t) - K_z^2 - \gamma/4}{K_\perp(t)} \right)''$$

$$\Delta\omega_g^2(K_y, K_z, t) \equiv \frac{K_\perp(t)}{\omega_g^2(t) - \omega_s^2(t)} \left(\frac{\omega_g^2(t) - K_z^2 - \gamma/4}{K_\perp(t)} \right)''$$

(here and below primes denote the time derivative). Note that all the time derivatives in these coefficients are proportional to the shear parameter q as well as to the azimuthal wavenumber K_y (time enters through $qK_y t$)

and thus vanish in the shearless limit $q = 0$ or in the case of axisymmetric perturbations with $K_y = 0$, reducing equations (30) and (31) to decoupled equations (29). In vertically stratified Keplerian discs, the dynamics of axisymmetric perturbations (modes) was extensively studied in the past (Ruden et al. 1988; Kley et al. 1993; Lubow & Pringle 1993; Korycansky & Pringle 1995; Ogilvie 1998; Mamatsashvili & Rice 2010), so we omit them from the present analysis and concentrate only on non-axisymmetric perturbations having non-zero azimuthal wavenumber $K_y \neq 0$, which we assume to be positive ($K_y > 0$) throughout without loss of generality.

Equations (30) and (31) describe the linear dynamics of the SDW and inertia-buoyancy modes and their coupling in a vertically stratified, compressible disc with (Keplerian) differential rotation. As mentioned above, novel features in the mode dynamics, in comparison with the case of no shear, arise from the coefficients $f_s, \Delta\omega_s^2$ and $f_g, \Delta\omega_g^2$ that originate from shear. The homogeneous (left-hand side) parts of equations (30) and (31) describe the individual behaviour of the SDW and inertia-buoyancy modes, respectively, in the presence of shear. The most interesting aspect here is the source terms on the right-hand side of these equations that provide coupling between these two modes. In other words, initially imposed only one mode acts as a source for another mode and can excite it in the course of evolution. Thus, the shear of disc flow introduces a phenomenon of mode conversion. We will see below that because of such a coupling, the convective and SDW modes actually have strictly separate identities only at large times ($|t| \gg 1$), when the characteristic time-scales (frequencies/growth rates) of these modes differ significantly (Fig. 1). As seen from Fig. 1, for finite times ($|t| \lesssim 1$) instead the mode time-scales are comparable and, as a result, the modes cannot be quite disentangled from each other, so that we have some mixture – ‘convective-SDW’ – mode at such times. If there was not such a difference in the SDW and convective modes’ time-scales, strictly speaking, it also would not make much sense to talk about homogeneous and particular inhomogeneous solutions of equations (30) and (31) separately, which themselves constitute a homogeneous system. Below, we will demonstrate using numerical analysis how the linear mode coupling occurs in practice.

For the purpose of numerical integration presented below, we change the eigenfunctions to $\Psi_s = \psi_s/h_s$, $\Psi_g = \psi_g/h_g$, where

$$h_s = \exp\left(-\frac{1}{2} \int_0^t f_s dt'\right), \quad h_g = \exp\left(-\frac{1}{2} \int_0^t f_g dt'\right).$$

These new eigenfunctions are more convenient, because substituting them into equations (30) and (31), we arrive at a simpler system without first derivatives on the left hand side

$$\frac{d^2 \Psi_s}{dt^2} + \hat{\omega}_s^2 \Psi_s = \chi_{sg1} \frac{d\Psi_g}{dt} + \chi_{sg2} \Psi_g, \quad (32)$$

$$\frac{d^2 \Psi_g}{dt^2} + \hat{\omega}_g^2 \Psi_g = \chi_{gs1} \frac{d\Psi_s}{dt} + \chi_{gs2} \Psi_s. \quad (33)$$

Equations (32) and (33) with time-dependent (modified) frequencies

$$\hat{\omega}_s^2 = \omega_s^2 + \Delta\omega_s^2 - \frac{f'_s}{2} - \frac{f_s^2}{4},$$

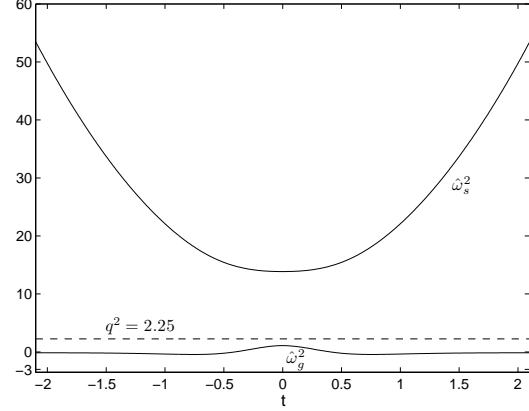


Figure 1. Modified frequencies $\hat{\omega}_s^2$ and $\hat{\omega}_g^2$ as functions of time at $K_y = 2$, $K_z = 3$ for the convectively unstable stratification with $\gamma = 0.8$. For comparison, with dashed line we also show the square of the inverse shear (non-dimensional) time $q^2 = 2.25$. In the vicinity of $t = 0$, all these three time-scales become comparable, whereas at large times they get separated: $\hat{\omega}_s^2$ increases as $\propto t^2$ and $\hat{\omega}_g^2$ tends to constant $N_0^2 = -0.25$.

$$\hat{\omega}_g^2 = \omega_g^2 + \Delta\omega_g^2 - \frac{f'_g}{2} - \frac{f_g^2}{4},$$

respectively, for the SDW and inertia-buoyancy modes, resemble equations of two coupled oscillators. These frequencies differ from corresponding ω_s^2 and ω_g^2 due to the presence of the shear-induced terms. For large times as well as for $K_y \gg 1$ and/or $K_z \gg 1$, these terms are small and $\hat{\omega}_s^2$ and $\hat{\omega}_g^2$ go to corresponding values in the shearless limit:

$$\hat{\omega}_s^2(t) \simeq K_{\perp}^2(t) + K_z^2,$$

$$\hat{\omega}_g^2(t) \simeq \frac{N_0^2 K_{\perp}^2(t) + \kappa^2(t)(K_z^2 + \gamma/4)}{K_{\perp}^2(t) + K_z^2}.$$

The χ parameters, describing the coupling between the modes, are given by

$$\chi_{sg1} = \frac{f_g h_g}{h_s}, \quad \chi_{sg2} = \frac{h_g}{h_s} \left(\Delta\omega_g^2 - \frac{f_g^2}{2} \right),$$

$$\chi_{gs1} = \frac{f_s h_s}{h_g}, \quad \chi_{gs2} = \frac{h_s}{h_g} \left(\Delta\omega_s^2 - \frac{f_s^2}{2} \right).$$

The coupling parameters χ_{sg1}, χ_{sg2} describe the excitation of the SDW mode by the inertia-buoyancy mode, while χ_{gs1}, χ_{gs2} describe the excitation of the inertia-buoyancy mode by the SDW mode. Figure 2 shows the temporal variation of the coupling parameters during the swing of a perturbation SFH from leading to trailing in the case of superadiabatic stratification with our chosen $\gamma = 0.8$. Accordingly, from now on we speak only of the convective mode instead of the more general inertia-buoyancy mode. In this case, $\hat{\omega}_g^2(t)$ has a negative sign for most of the time (Fig. 1) and determines the shear-modified instantaneous growth rate of convective instability. It is seen from Fig. 2 that for fixed K_y and K_z , these parameters reach their maximal values in the interval $|t| \lesssim 1$, when the time-dependent radial wavenumber is not large, $|K_x(t)/K_y| = q|t| \lesssim 1$, and rapidly decay at $|t| \gg 1$, when $|K_x(t)/K_y| = q|t| \gg 1$ as well. Thus,

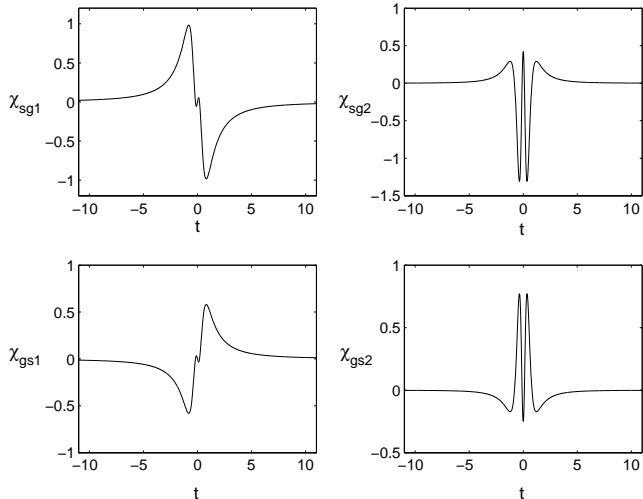


Figure 2. Coupling parameters χ as a function of time for $K_y = 2$, $K_z = 3$. They reach the highest values during $|t| \lesssim 1$ and fall off at large times $|t| \gg 1$.

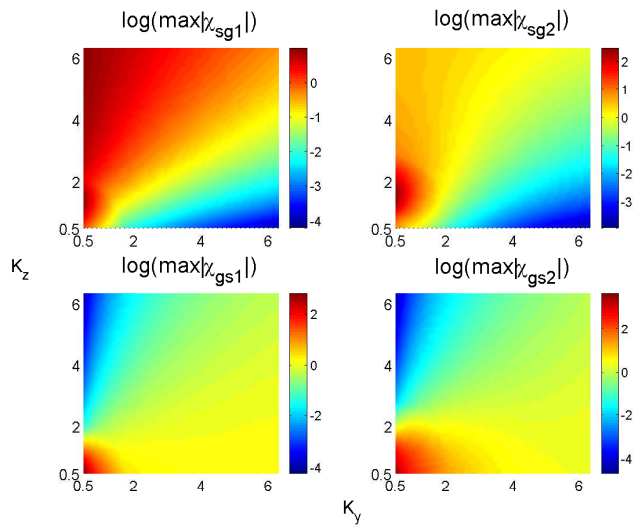


Figure 3. Maximum values of modulus of coupling parameters, $|\chi|$, as a function of K_y and K_z . $\max|\chi_{sg1}|$ and $\max|\chi_{sg2}|$ are appreciable over a broader range of wavenumbers than $\max|\chi_{gs1}|$ and $\max|\chi_{gs2}|$.

because the coupling parameters χ evidently also originate from shear, we can conclude that at given K_y and K_z , the influence of shear on the mode dynamics can be important only for moderate radial wavenumbers and an efficient energy exchange between the modes and the mean disc flow should be expected to occur just during this interval, which we will call a coupling interval. For $|K_x(t)/K_y| \gg 1$, the coupling parameters are small and hence the modes become dynamically decoupled from each other and evolve independently (see the next section). In Fig. 3, the maximal values (over the interval $|K_x(t)/K_y| \lesssim 1$) of the modulus of the coupling parameters are plotted in the (K_y, K_z) -plane. The maximum values of $|\chi_{sg2}|$, $|\chi_{gs1}|$ and $|\chi_{gs2}|$ are appreciable for of the order of unity or smaller K_z , K_y and rapidly decay with the increase of these wavenumbers. The maximum of

$|\chi_{sg1}|$ is appreciable over a broader range of wavenumbers, but it has larger values at smaller K_y . Because the coupling parameters are generally one of the factors determining the generation of one mode by another, we should expect the efficiency of coupling of the SDW and convective modes as a function of K_y and K_z to follow, to a certain extent, the same trend as that of the coupling parameters shown in Fig. 3. Although in a superadiabatically stratified disc the generation (triggering) of convective motions by SDWs, determined by the coupling parameters χ_{gs1}, χ_{gs2} , is in principle possible, here we focus only on excitation of SDWs by convection, determined by χ_{sg1}, χ_{sg2} , as it seems more interesting. Besides, convection can be easily triggered by other mechanisms in discs.

3 SDW AND CONVECTIVE MODES – SHEAR-INDUCED COUPLING

In this section, we study the shear-induced dynamics of the non-axisymmetric SDW and convective modes by numerically solving equations (32) and (33). At large times/radial wavenumbers ($|K_x(t)/K_y| = q|t| \gg 1$), the adiabatic (WKB) condition with respect to time is satisfied for the mode frequency/growth rate,

$$|\dot{\omega}'_{s,g}(t)| \ll |\dot{\omega}^2_{s,g}(t)|.$$

A physical interpretation of this inequality is that the time-scale of shear-induced variation of the frequency/growth rate is much larger than the characteristic time-scale (i.e., inverse frequency/growth rate) of the mode itself. In this adiabatic regime, $\dot{\omega}^2_g(t) \simeq N_0^2 < 0$, so it is nearly independent of time and is much less than the frequency of SDWs, which increases linearly with time, $\dot{\omega}_s(t) \simeq K(t) \approx qK_y|t| \gg 1$, so that the mode time-scales are well separated (Fig. 1). In addition, all four coupling parameters χ are negligible at these times (Fig. 2). These imply that in the adiabatic regime, shear plays only a minor role in the dynamics of SDWs and convective instability. Below we will refer to this asymptotic stage as adiabatic/non-coupling region in the \mathbf{K} -space. Consequently, if the convective mode is in the adiabatic region, it will evolve with time as in the shearless limit, without any exchange of energy and exciting other modes (i.e., SDWs) in the disc. However, if $K_x(t)$ crosses the coupling interval $|K_x(t)/K_y| \lesssim 1$ during its drift, where, as we have seen, the influence of shear on the mode dynamics becomes significant, the excitation of SDWs by non-axisymmetric convective motions can take place. So, the goal of this section is to examine this phenomenon in detail.

For further use, we also introduce the mode energies as

$$E_s \equiv |\Psi'_s|^2 + \dot{\omega}_s^2(t)|\Psi_s|^2, \quad E_g \equiv |\Psi'_g|^2 + \dot{\omega}_g^2(t)|\Psi_g|^2.$$

for the SDW and convective modes, respectively. In the absence of shear they are conserved quantities, as it follows from equations (29). The mode energies are useful in characterising mode dynamics for asymptotically large times, in the adiabatic regime. In this regime, the energies vary with time due solely to the mean shear flow. In particular, the SDW mode energy grows linearly with time,

$$E_s \propto \dot{\omega}_s(t) \simeq K(t) \propto |t|,$$

which follows from equation (32) in the WKB regime neglecting the coupling parameters, which are small in this

regime anyway. Such an asymptotic behaviour of the SDW mode energy will later prove to be a useful diagnostic in analysing the generation of SDWs. Note also that at large times E_s is obviously positive definite, whereas E_g can become negative (Fig. 4), since $\hat{\omega}_g^2 \simeq N_0^2 < 0$ at these times.

3.1 Generation of the SDW mode by the convective mode

We wish to investigate the convective instability in the presence of Keplerian shear and, specifically, how convective motions can excite SDWs. To this end, initially at $t = -t_0$, where $t_0 \gg 1$ is some large positive parameter, we impose a tightly leading (i.e., with $K_x(-t_0)/K_y \ll -1$) SFH of the convective mode on the flow without any mixture of a SDW mode SFH and follow the subsequent evolution of the eigenfunctions and perturbed quantities until $t = t_0$, at which stage their SFHs become tightly trailing (with $K_x(t_0)/K_y \gg 1$). For numerical integration we use a standard Runge-Kutta scheme (MATLAB ode45 RK implementation).

To prepare such initial conditions, we make use of the fact that at $t \ll -1$ the dynamics is adiabatic and the modes do not interact with each other that, in turn, permits us to pick out (impose) only the convective mode at the beginning. In this adiabatic/non-coupling regime, the convective mode is given by the WKB asymptotic solution of the homogeneous part of equation (33), which we take to have the form

$$\Psi_g = \frac{C_0}{\sqrt{|\hat{\omega}_g(t)|}} \exp\left(\int_{-t_0}^t |\hat{\omega}_g(t')| dt'\right) \quad \text{at } t \ll -1, \quad (34)$$

where C_0 is a some arbitrary constant setting the initial value of Ψ_g at the start of integration at $t = -t_0$. This solution means that the convective mode is evanescent in the distant past (at $t \rightarrow -\infty$) and grows with time afterwards. As for the initial value of the SDW mode eigenfunction, a high-frequency SDW component is absent at the outset, so that Ψ_s should be given only by non-oscillatory particular solution, $\Psi_s^{(g)}$, of equation (32) coming from the source term on the right hand side that is associated with the convective mode. Asymptotically at $t \ll -1$, we can ignore the second order time derivative in equation (32) and represent the initial value of Ψ_s at these times, to a good approximation, as

$$\Psi_s = \Psi_s^{(g)} \approx \frac{\chi_{sg1} \Psi_g' + \chi_{sg2} \Psi_g}{\hat{\omega}_s^2(t)}. \quad (35)$$

Indeed, as mentioned above, in the adiabatic regime, (i) the period of the SDW oscillations is much smaller than the shear/dynamical time, or equivalently $|\hat{\omega}_s'| \ll \hat{\omega}_s^2$, (ii) the coupling parameters vary a little during the oscillation period and at the same time (iii) the frequency of SDWs is much larger than the characteristic growth rate of the convective mode, $|\hat{\omega}_g| \ll \hat{\omega}_s$. As a result, the second time derivative of the particular solution (35) turns out to be much smaller than the right hand side term of equation (32), thereby validating our approximation. This slowly varying solution ensures that the oscillatory SDW mode is absent in the initial conditions. Note also that as the coupling coefficients are vanishing at $t \rightarrow -\infty$, we also have $\Psi_s^{(g)}(-\infty) \rightarrow 0$, $\Psi_s^{(g)'}(-\infty) \rightarrow 0$. This in fact coincides with

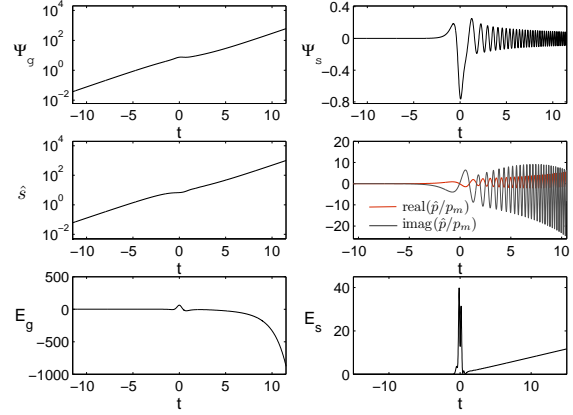


Figure 4. Evolution of the eigenfunctions Ψ_g and Ψ_s , entropy \hat{s} , normalised perturbed pressure \hat{p}/p_m and corresponding energies E_g, E_s pertaining to an initially imposed purely convective mode SFH with $K_y = 2, K_z = 3$. At the beginning, Ψ_g and \hat{s} evolve adiabatically, exponentially growing with the characteristic growth rate $|\hat{\omega}_g|$, while Ψ_s and \hat{p} are still nearly zero. At around $t = 0$, rapid oscillations abruptly emerge in the evolution of Ψ_s and \hat{p} that indicate a trailing SFH of the SDW mode being excited. In addition, the convective mode causes \hat{p} to grow as well while oscillating. Accordingly, the energy of the SDW mode, E_s , being negligible at $t < 0$, after the transient amplification event in the vicinity of $t = 0$, increases linearly with time in the subsequent adiabatic regime at $t \gg 1$ (which actually starts already at $t \sim 1$).

the condition of the absence of SDWs in the shearless limit. Thus, asymptotic solutions (34) and (35) can be viewed as a generalisation of the recipe for imposing only the convective mode, without a mixture of SDWs, on the flow in the absence of shear (i.e., $\Psi_s(-\infty) = \Psi_s'(-\infty) = 0$) to the case of non-zero shear provided, however, that the adiabatic approximation is still met, which is always the case at large times.

Figure 4 shows the subsequent temporal evolution corresponding to initial conditions/solutions (34) and (35). Together with the eigenfunctions, which more clearly illustrate mode coupling, we also plot the time-development of the perturbed entropy \hat{s} , normalised pressure \hat{p}/p_m and mode energies E_g and E_s . At the beginning, while the convective mode SFH is still in the adiabatic region $K_x(t)/K_y = qt \ll -1$ and far from the coupling region, the eigenfunction Ψ_g , following expression (34), grows exponentially with the instantaneous growth rate $|\hat{\omega}_g|$ and induces a similar behaviour in the entropy, whereas Ψ_s , evolving according to (35), still remains very small and non-oscillatory. The evolution of the corresponding energy E_s is similar to that of Ψ_s . It is also seen in Fig. 4 that at this initial adiabatic stage of evolution, the entropy perturbation is dominant over the pressure perturbation, which, like Ψ_s , is small and aperiodic initially. It can also be shown that the form of our initial conditions for the convective mode implies $E_g = 0$ at $t \ll -1$, because of the negative $\hat{\omega}_g^2 < 0$; of course, this does not mean that the convective mode is zero.

As time passes, the time-dependent radial wavenumber $K_x(t)$ of the convective mode SFH gradually approaches the coupling region $|K_x(t)/K_y| \lesssim 1$ and begins to cross it. In this region, the effects of shear come into play: the coupling

parameters become appreciable (Fig. 2) and simultaneously the characteristic time-scales of the SDW mode, convective mode and the shear time ($= 1/q$ in the non-dimensional form) become comparable,³ or equivalently $q \sim |\hat{\omega}_g| \sim \hat{\omega}_s$ (Fig. 1), also implying that in the coupling region, the adiabatic condition for the SDW frequency breaks down, $|\hat{\omega}'_s| \sim |\hat{\omega}_s^2|$, that is, the coupling region is also non-adiabatic. This results in an efficient energy exchange between these two modes and the background shear flow in this coupling region. First, at $-1 \lesssim t < 0$, the eigenfunction Ψ_s , pressure \hat{p} and the energies E_g, E_s undergo transient amplification by extracting energy mainly from the background flow, but still remain aperiodic. The evolution of Ψ_s has now deviated from the asymptotic solution (35), because the second derivative of Ψ_s has become important in equation (32), though it is still following non-oscillatory $\Psi_s^{(g)}$. Then, during a short period of time around $t = 0$, when $K_x(t)$ crosses the point $K_x = 0$, swinging from negative (leading) to positive (trailing), rapid oscillations abruptly appear in the evolution of Ψ_s and the pressure, signaling the generation of a trailing SFH of the SDW mode. So, now at $t > 0$, there are the newly excited trailing SDW mode SFH and the former convective mode SFH. It can be said that the convective mode, in some sense, acts as a mediator between SDWs and the disc shear flow. The energy needed for the SDW excitation is mainly extracted from the shear with the help of the convective mode. We would also like to note that, as mentioned above, because the time-scales of the convective and excited SDW modes are comparable, strictly speaking, these modes cannot be well distinguished from each other in the coupling region. In other words, we have a mixture – ‘convective-SDW’ mode – at intermediate times, $|t| \lesssim 1$. Then, on leaving the coupling region, $K_x(t)$ moves into the next adiabatic region $K_x(t)/K_y \gg 1$ where the linear dynamics of SDWs and convection become decoupled with no further energy exchange, so the modes thus acquire truly separate identities. The mode time-scales has now been separated (Fig. 1): the pressure \hat{p} rapidly oscillates as a result of the new SDW component in Ψ_s with the frequency $\hat{\omega}_s(t)$, which increases linearly with time and soon becomes much larger than the growth rate, $|\hat{\omega}_g|$, of the convective instability. The eigenfunction Ψ_g continues to grow exponentially with this growth rate and causes a similar growth in the entropy. As typical of SDWs in the adiabatic regime, the corresponding energy E_s increases linearly with time solely due to the background flow.

Finally, we would like to stress again that the studied here linear coupling of the SDW and convective modes caused by shear is essentially of the same nature as other linear mode coupling phenomena occurring in disc flows with Keplerian shear: coupling of vortical and wave modes, that is, the generation of SDWs by vortices (Bodo et al. 2005; Johnson & Gammie 2005a; Mamatsashvili & Chagelishvili 2007, HP09a), coupling of vortices and inertia-gravity waves (Tevzadze et al. 2003, 2008) and coupling of baroclinic and SDW modes (Tevzadze et al. 2010). Thus, the linear mode

coupling is a generic phenomenon inevitably taking place whenever the mean flow is inhomogeneous (i.e., the velocity profile has a non-zero shear) and all these cases are its special manifestations for particular physical settings. In this connection, we should mention that it also occurs in MHD shear flows, where in general there are larger number of mode branches with different time-scales and coupling among them becomes quite complex (Chagelishvili et al. 1996). For example, Heinemann & Papaloizou (2009b) described the generation of SDWs by the vortical mode in a MRI-turbulent disc shear flow. The coupling among different MHD modes can also be seen in the linear analysis of non-axisymmetric MRI by Balbus & Hawley (1992), however, the authors do not identify it as such. Thus, the primary effect of shear of the disc’s differential rotation on the perturbations dynamics is that it couples, or introduces a new channel of energy exchange among different types of perturbation modes existing in the disc as well as with the disc flow. In the present case, the linear dynamics of the convective mode is accompanied by the generation of high-frequency SDWs during a finite-time interval as SFHs swing from leading to trailing. As noted before, the shearing wave (non-modal) approach, because of not involving spectral expansion in time, allows us to trace an entire temporal evolution of perturbations and thus to reveal new aspects of non-axisymmetric convection in disc shear flows. This, in turn, can provide further insight into the role of convection and its coupling with SDWs in angular momentum transport, especially now when the capability of convection to transport angular momentum outwards in discs has recently been established via numerical simulations (we address the transport properties of the modes in section 4). Previous linear studies of non-axisymmetric convection have been either in the framework of the modal approach (Lin et al. 1993) or using the shearing wave (non-modal) approach (RG92; Korycansky 1992; Brandenburg & Dinnis 2006) as here, but without identification and characterisation of the mode coupling process. As pointed out in the Introduction, the results of the modal approach are actually applicable for asymptotically large times and therefore tend to overlook dynamical effects at intermediate times arising as a result of the flow non-normality/shear. Since the excitation of SDWs by convection is just one of such examples occurring during a limited time interval, in fact it cannot be captured in the framework of the modal approach.

3.2 Generation of SDWs for various K_y and K_z

Here we examine how the efficiency of the above-described SDW generation process depends on the azimuthal, K_y , and vertical, K_z , wavenumbers. Figure 5 shows the evolution of Ψ_s under the same initial conditions (34) and (35) as above, that is, consisting of an initially imposed only tightly leading convective mode SFH at various K_y and K_z , without a mix of the SDW mode SFH. For large K_y and/or K_z (i.e., when the azimuthal and/or vertical wavelengths of the modes are much smaller than the disc scale height), starting out with very small values, Ψ_s mainly undergoes only transient variation in the coupling region (at $|t| \lesssim 1$) followed by very weak, almost no generation of high-frequency oscillations, i.e., SDW component. The reason for such a behaviour is the following. At large K_y and/or K_z , the time-scales of

³ This is not the case at large K_y and/or K_z , because the mode time-scales still remain separated even for $|K_x(t)/K_y| \lesssim 1$ and therefore the mode coupling is negligible at large wavenumbers; see section 3.2.

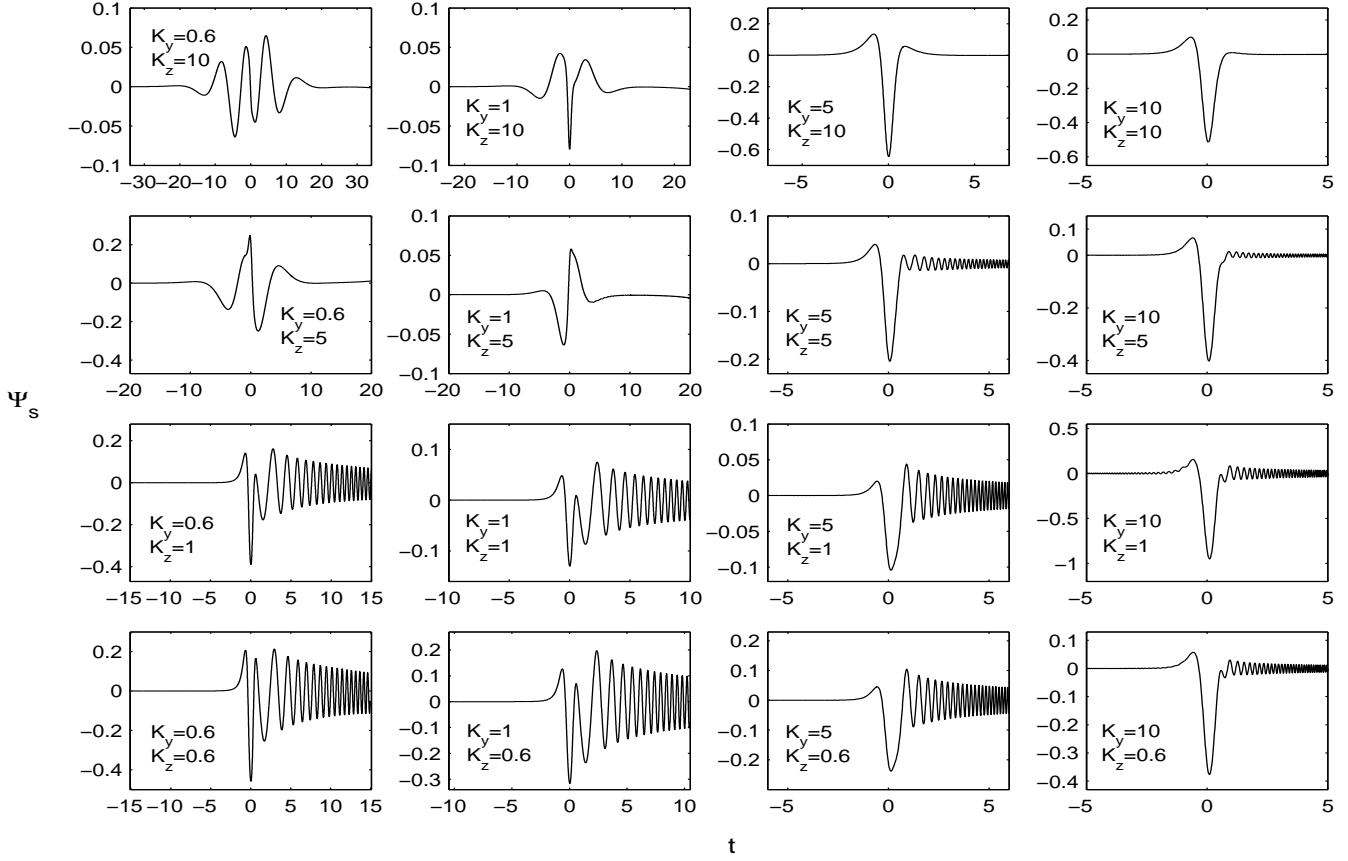


Figure 5. Evolution of Ψ_s corresponding to an initially imposed convective mode SFHs with various K_y and K_z . Appreciable oscillations in the time-development of Ψ_s appear and, therefore an efficient SDW mode excitation occurs, at $K_y, K_z \lesssim 1$. By contrast, at large K_y and/or K_z , Ψ_s undergoes only small transient variation (growth) in the interval $|t| \lesssim 1$ with very weak, almost no SDW generation.

the SDW and convective modes remain well separated during an entire course of evolution, not only at large times, and the adiabatic condition for the SDW frequency holds. As a result, non-oscillatory particular solution (35), valid for the initial adiabatic stage of evolution at $t \ll -1$, in fact continues to hold at all times to a good approximation (because its second time derivative always remains negligible in equation 32) and, consequently, an efficient coupling between the SDW and convective modes is not feasible at large K_y and/or K_z . So, in Fig. 5, the time-development of Ψ_s at these wavenumbers is given by this particular solution which does not involve any oscillations. (To be more precise, the SDW mode is still being generated, but with a very small, as evident from the panels with $K_y = 5, K_z = 5$; $K_y = 10, K_z = 5$; $K_y = 10, K_z = 1$; $K_y = 10, K_z = 0.6$ of Fig. 5 and also from Fig. 6.) Thus, the regime of large azimuthal and/or vertical wavenumbers is a weak coupling regime, where shear plays only a minor role in the mode dynamics. By contrast, for smaller $K_y, K_z \lesssim 1$ (i.e., for wavelengths comparable to the disc scale height) the favourable conditions for mode coupling – violation of the adiabatic condition and comparable time-scales of the SDW and convective modes and the shear time – can occur in the vicinity of $t = 0$, leading to an efficient generation of the SDW mode by the convective one, as described in section 3.1.

We can quantitatively characterise the mode coupling as follows. At $t > 0$, the total solution for Ψ_s consists of the

two components

$$\Psi_s = \Psi_s^{(w)} + \Psi_s^{(g)},$$

where $\Psi_s^{(g)}$, as before, is the non-oscillatory, slowly varying particular solution of equation (32) due to the convective mode and $\Psi_s^{(w)}$ is an oscillatory component related to the SDW mode generated by this particular solution. So, the relative intensity of the wave generation process can be quantified by comparing the value of $\Psi_s^{(w)}$ to that of $\Psi_s^{(g)}$. To do this, we introduce the parameter

$$\epsilon \equiv \frac{\max_{t>0} |\Psi_s^{(w)}(t)|}{\max_{t>0} |\Psi_s^{(g)}(t)|},$$

which is the ratio of the maximal values of $|\Psi_s^{(w)}|$ and $|\Psi_s^{(g)}|$ over time (typically, both these functions achieve their maximal values in the vicinity of $t = 0$, as seen in Fig. 5). Obviously, with our initial conditions (34) and (35), this ratio does not depend on the arbitrary parameter C_0 and is a function of K_y and K_z only, which is plotted in Fig. 6. It is seen from this figure that at large K_y and/or K_z , as expected, $\epsilon \lesssim 0.1$ is small, implying that the non-oscillatory particular solution dominates over the oscillatory SDW mode solution, i.e., wave generation is weak. For $K_y, K_z \lesssim 1$, $\epsilon \sim 1$ implying that the wave component is comparable to the non-oscillatory solution and therefore the SDW generation is appreciable. This also confirms the situation in Fig. 5.

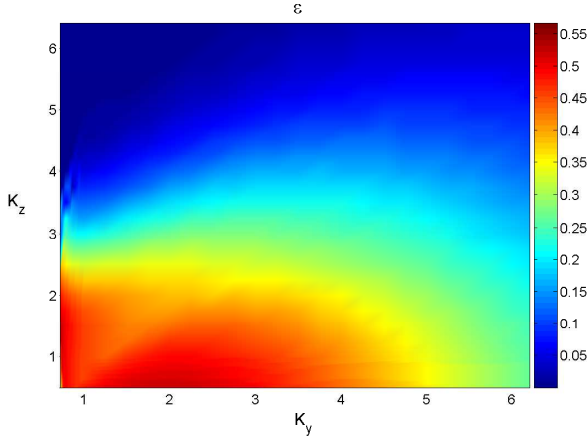


Figure 6. Ratio, ϵ , of the maximum values of the SDW mode solution to its generator non-oscillatory particular solution of equation (32) due to the convective mode, plotted as a function of K_y and K_z .

3.3 Amplitudes of generated SDWs

We can go further and calculate the amplitudes of SDWs generated by the convective mode, which also represent a measure of the coupling efficiency between these two modes. In this section, we choose the constant C_0 in the WKBJ solution (34), describing an initially tightly leading convective mode SFH at $t \ll -1$, such that to have

$$\Psi_g = \frac{C_0}{\sqrt{|\hat{\omega}_g(t)|}} \exp\left(\int_{-t_0}^t |\hat{\omega}_g(t')| dt'\right) = \frac{1}{\sqrt{|N_0|}} e^{|N_0|t}.$$

An advantage of this form is that the calculated below SDW amplitudes depend only on K_y and K_z and are independent of the choice of the starting point $-t_0$ (as long as $t_0 \gg 1$). In this initial adiabatic regime, as before, $\Psi_s = \Psi_s^{(g)}$, because SDWs are absent at the outset. Then, in the non-adiabatic region at $|t| \lesssim 1$, the mode coupling is at work and subsequently, at around $t = 0$, the SDW mode SFH abruptly emerges. After crossing the non-adiabatic/coupling region, in the next adiabatic region at $t \gg 1$, there are the former convective mode SFH and the generated by it SDW mode SFH, both with tightly trailing orientation. So, now, as noted above, the full solution for Ψ_s is the sum of the following parts:

$$\begin{aligned} \Psi_s &= \Psi_s^{(w)} + \Psi_s^{(g)} = \\ &= \frac{A}{\sqrt{\hat{\omega}_s(t)}} \exp\left(-i \int_0^t \hat{\omega}_s(t') dt'\right) + \\ &+ \frac{A^*}{\sqrt{\hat{\omega}_s(t)}} \exp\left(i \int_0^t \hat{\omega}_s(t') dt'\right) + \\ &+ \frac{\chi_{sg1} \Psi_g' + \chi_{sg2} \Psi_g}{\hat{\omega}_s^2(t)} \quad \text{at } t \gg 1, \end{aligned}$$

where the first two terms are oscillatory WKBJ solutions of the homogeneous part of equation (32) that correspond to the excited SDWs. Since the initial conditions are real, these solutions come in complex conjugate pairs with different signs of frequency and with amplitudes A and its complex conjugate A^* . Thus, the SDW mode SFH generated by the convective mode is actually a superposition of two SFHs

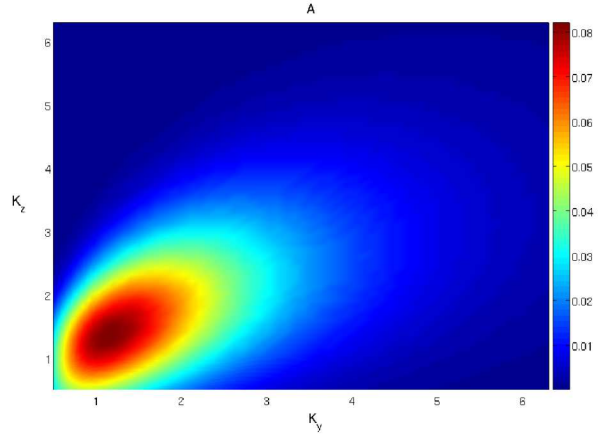


Figure 7. Absolute value of the amplitude, $|A|$, of SDWs generated by the convective mode as a function of K_y and K_z . It achieves the largest value $|A|_{max} = 0.082$ at $K_{y,m} = 1.2, K_{z,m} = 1.3$ and decreases at smaller and larger K_y, K_z , implying also the decrease in the mode coupling efficiency at these wavenumbers.

corresponding to SDWs propagating in opposite directions. In other words, convection always pairwise excites SDWs that propagate oppositely, similar to SDWs generated by the vortical mode in 2D discs (see e.g., HP09a). The third term is again the non-oscillatory slowly varying particular solution due to the convective mode.

Figure 7 shows the dependence of the absolute value of the amplitude, $|A|$, on K_y and K_z . When either of these wavenumbers is large, $|A|$ is small, because, as shown above, the SDW generation/mode coupling is inefficient. With decreasing K_y and K_z , as expected, the amplitude increases and attains its maximum values at $K_y, K_z \lesssim 1$, because an appreciable SDW generation takes place at such wavenumbers, as seen in Figs. 5 and 6. Note that $K_y, K_z \lesssim 1$ is the region where the coupling parameters χ_{sg1}, χ_{sg2} are appreciable too (see Fig. 3). Comparing Figs. 6 and 7, we also see that the amplitude $|A|$ and ϵ , which is a measure of the mode coupling efficiency, behave with K_y and K_z more or less similarly.

4 ANGULAR MOMENTUM TRANSPORT BY THE CONVECTIVE AND SDW MODES

In this section, we analyse the angular momentum transport properties of the SDW and convective modes. Specifically, we are interested in the radial component of angular momentum flux carried by these two modes, because it determines the radial transport of mass and hence accretion onto the central star. The angular momentum conservation law for linear perturbations in the shearing box model follows from the invariance of the system under translations in the azimuthal y -direction. It can be derived by application of Noether's theorem to the second order Lagrangian density (RG2; HP09a; Narayan et al. 1987)

$$\begin{aligned} L &= \frac{\rho_0}{2} \left(\frac{D\xi}{Dt}\right)^2 - \frac{p_0}{2} \left[(\gamma - 1)(\nabla \cdot \xi)^2 + \frac{\partial \xi_i}{\partial x_j} \frac{\partial \xi_j}{\partial x_i}\right] + \\ &+ \rho_0 (\Omega \times \xi) \cdot \frac{D\xi}{Dt} + q\rho_0 \Omega^2 \xi_x^2, \end{aligned}$$

in this direction and yields

$$\frac{D}{Dt} \left(\frac{\partial L}{\partial(D\xi_i/Dt)} \frac{\partial \xi_i}{\partial y} \right) + \frac{\partial}{\partial x_j} \left(\frac{\partial L}{\partial(\partial \xi_i / \partial x_j)} \frac{\partial \xi_i}{\partial y} - L \delta_{j2} \right) = 0,$$

where ξ is the displacement vector related to the perturbed velocity by

$$u_x = \frac{D\xi_x}{Dt}, \quad u_y = \frac{D\xi_y}{Dt} + q\Omega\xi_x, \quad u_z = \frac{D\xi_z}{Dt},$$

and δ_{ij} is the Kronecker delta and the summation is assumed over the repeated indices $i, j = 1, 2, 3$ corresponding to $(x_1, x_2, x_3) \equiv (x, y, z)$. (It can also be readily shown that this Lagrangian density through variation gives the original set of linear perturbation equations 9-13). Since we are mainly concerned with the radial x -component of the angular momentum flux, we can average this equation over both y - and z -coordinates. After averaging, the canonical angular momentum density in brackets in the first term, as demonstrated by Narayan et al. (1987), actually coincides with the density of the radial component of true physical angular momentum, but taken with the minus sign and without fiducial radius r_0 that does not play any role in the local analysis. So, we write for the radial component, B , of angular momentum density

$$B = - \left\langle \frac{\partial L}{\partial(D\xi_i/Dt)} \frac{\partial \xi_i}{\partial y} \right\rangle_{yz},$$

where the angle brackets denote averaging over y and z . On similarly averaging the second term and taking it with the minus sign, we obtain the desired radial component of the angular momentum flux

$$F_x = - \left\langle \frac{\partial L}{\partial(\partial \xi_i / \partial x)} \frac{\partial \xi_i}{\partial y} \right\rangle_{yz} = - \left\langle p' \frac{\partial \xi_x}{\partial y} \right\rangle_{yz},$$

where the pressure perturbation p' (as used in equations 9-13, the prime is not time-derivative in this case) is related to the displacement vector through $p' = -\rho_0 c_s^2 \nabla \cdot \xi + \rho_0 g \xi_z$. After that the angular momentum conservation takes more compact form

$$\frac{\partial B}{\partial t} + \frac{\partial F_x}{\partial x} = 0.$$

For the angular momentum flux associated with an individual SFH given by (15) and (16) after spatial averaging we get

$$F_x = \frac{i}{4} K_y [\hat{p}(t) \hat{\xi}_x^*(t) - \hat{\xi}_x(t) \hat{p}^*(t)],$$

where again $\hat{p}(t)$ and $\hat{\xi}_x(t)$ are the amplitudes of SFHs depending only on time with $\hat{p}^*(t)$ and $\hat{\xi}_x^*(t)$ being their respective complex conjugates. The velocity and displacement amplitudes are related by $\hat{u}_x(t) = d\hat{\xi}_x(t)/dt$. We normalise displacement ξ as other scale-lengths above, $\Omega\xi/c_s \rightarrow \xi$, and pressure and flux as $\hat{p}/p_m \rightarrow \hat{p}$, $F_x/p_m \rightarrow F_x$. Since, we have two modes – SDWs and convection, we decompose \hat{p} and $\hat{\xi}_x$ into two parts corresponding to these modes

$$\hat{p} = \hat{p}_s + \hat{p}_g, \quad \hat{\xi}_x = \hat{\xi}_{x,s} + \hat{\xi}_{x,g},$$

where \hat{p}_s and $\hat{\xi}_{x,s}$ are related to the SDW component and, therefore, are rapidly oscillating in time with the frequency of the latter, while \hat{p}_g and $\hat{\xi}_{x,g}$ are related to the convective

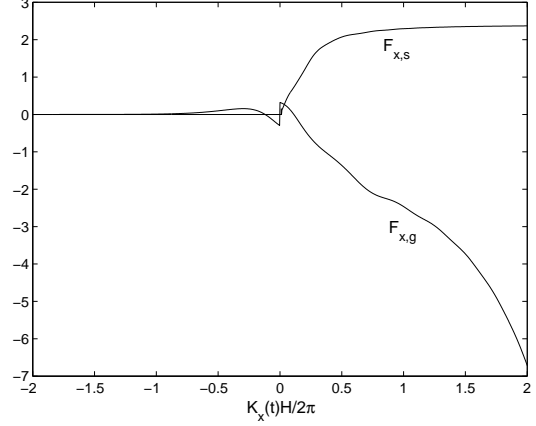


Figure 8. Radial angular momentum fluxes associated with the convective mode, $F_{x,g}$, and with the generated by it the SDW mode, $F_{x,s}$, for $K_{y,m} = 1.2$, $K_{z,m} = 1.3$. The jump of $F_{x,s}$ and $F_{x,g}$ in the immediate vicinity of $t = 0$ is due to the abrupt emergence of the SDW mode.

mode and vary on its corresponding time-scale, relatively slowly compared with the SDW mode. So, the total flux

$$F_x = \frac{i}{4} K_y [(\hat{p}_s + \hat{p}_g)(\hat{\xi}_{x,s}^* + \hat{\xi}_{x,g}^*) - (\hat{\xi}_{x,s} + \hat{\xi}_{x,g})(\hat{p}_s^* + \hat{p}_g^*)]$$

is also of oscillatory type because of the presence of the SDW mode, but we can conveniently smooth it by averaging over the oscillation period much smaller than the growth time of the convective mode (we denote the time-averaging with angle brackets without subscript). As a result, we have

$$F_x = \frac{i}{4} K_y \langle \hat{p}_s \hat{\xi}_{x,s}^* - \hat{\xi}_{x,s} \hat{p}_s^* \rangle + \frac{i}{4} K_y \langle \hat{p}_g \hat{\xi}_{x,g}^* - \hat{\xi}_{x,g} \hat{p}_g^* \rangle. \quad (36)$$

Thus, all the cross-products vanish after time-averaging and the total angular momentum flux appears as a sum of angular momentum fluxes

$$F_{x,s} = \frac{i}{4} K_y \langle \hat{p}_s \hat{\xi}_{x,s}^* - \hat{\xi}_{x,s} \hat{p}_s^* \rangle,$$

$$F_{x,g} = \frac{i}{4} K_y \langle \hat{p}_g \hat{\xi}_{x,g}^* - \hat{\xi}_{x,g} \hat{p}_g^* \rangle$$

related, respectively, to the SDW and convective modes (we have omitted the angle brackets in $F_{x,g}$, as it does not change much during the oscillation period). In an analogous calculation of the angular momentum transport by non-axisymmetric shearing waves, RG92 obtained a rapidly oscillating, on average negative, angular momentum flux and attributed it only to the convective mode without separating/analysing the contribution from SDWs. In fact, this contribution is present, because, as demonstrated here, SDWs are inevitably generated by the convective mode due to background shear. So, decomposition (36) allows us to analyse the angular momentum fluxes carried by each mode individually and contrast them.

In Fig. 8, we show the time-history of the fluxes $F_{x,s}$ and $F_{x,g}$ when a tightly leading purely convective mode SFH is imposed initially. At $t < 0$, before SDW mode generation, angular momentum transport is solely due to the convective

mode SFH and is still small and positive. Then, in the vicinity of $t = 0$, trailing SDW mode SFH emerges, giving rise to its associated flux $F_{x,s}$ at $t > 0$, which initially increases and soon settles to a positive and constant value. Thus, trailing SDWs always transport angular momentum outwards. (A similar result was also obtained by HP09a for SDWs generated by the vortical mode.) As for the angular momentum flux of the convective mode, during a short period of time after $t = 0$, it is still positive, but quickly switches to increasingly negative due to the exponential growth of Ψ_g , and dominates over the positive flux of the SDW mode with time. Because of the relatively short time-scale of the wave generation process in the immediate vicinity of $t = 0$, the variations of $F_{x,s}$ and $F_{x,g}$ also appear sharp around $t = 0$. However, as demonstrated by Lesur & Ogilvie (2010) and Käpylä et al. (2010), this flux of angular momentum associated with the convective mode, being negative in the linear regime, can actually change sign (direction) in the non-linear regime. We also see from Fig. 8 that shortly after the SDW mode generation, at $K_x(t)H/2\pi \lesssim 1$ (i.e., when the radial wavelength is still larger than or equal to the scale height), its corresponding flux, $F_{x,s}$, achieves a maximum value comparable to, though still less by absolute value, than that of the convective mode, $F_{x,g}$. As Heinemann & Papaloizou (2009b) showed, just these values of the angular momentum flux of SDWs during the time when their time-dependent $K_x(t)$ are still in the range $K_x(t)H/2\pi \lesssim 1$, are important and determine transport in the non-linear regime, because SDWs with radial wavenumbers larger than this are subsequently damped via shock formation in the trailing phase.⁴ Thus, SDWs generated by convection are, in principle, capable of fully contributing to the transport before undergoing significant damping. Based on this, in the non-linear regime, we may expect that the positive flux due to SDWs will aid and enhance the outward angular momentum transport due to the convective mode alone, although a further non-linear study is required to ascertain this.

5 SUMMARY AND DISCUSSION

In this paper, we have performed a detailed investigation of a new linear mechanism of spiral density wave excitation by vertical thermal convection in compressible Keplerian discs with superadiabatic vertical stratification, using the local shearing box approach. The wave excitation results from the velocity shear of the disc's Keplerian differential rotation. As is usually done in the shearing box, perturbations were decomposed into spatial Fourier harmonics, or shearing plane waves. The temporal evolution of the amplitudes of these waves was followed by numerical integration of the linearised hydrodynamical equations of the shearing box. Only non-axisymmetric perturbations were considered, as only for them the effects of shear are important. Three basic types of perturbation modes can be distinguished in the considered system: SDWs due mainly to compressibility, the convective mode due mainly to the negative vertical entropy gradient,

and the vortical mode due to the combined action of vertical stratification and the Coriolis force. However, in the present case of non-self-gravitating discs with superadiabatic vertical structure, the main energy-carrying mode is convection. In such a setup, the vortical mode can be neglected and hence we have concentrated primarily on the dynamics of SDWs and the convective mode, which both have zero potential vorticity. We first characterised the properties of the SDW and convective modes by deriving the dispersion relations in the presence of disc rotation and stratification, but neglecting shear of disc flow. In this limit of rigid rotation, the modes evolve independently, that is, once either of these modes has been initially excited, it does not lead to the excitation of another. We then demonstrated that on taking into account differential rotation/shear, an initially tightly leading SFH of the convective mode evolving in the disc flow, on becoming trailing, generates a corresponding SFH of SDWs. The main mechanism of wave generation is the following. Because of shear, the radial wavenumber of SFH varies with time, making the characteristic time-scales of these modes time-dependent as well. As a result, during a short period of time when SFHs swing from leading to trailing, the mode time-scales can become comparable to each other and to the shear time, thereby making an efficient energy exchange between the SDW mode, convective mode and the mean disc flow possible. Consequently, SDWs are generated in this process, mainly at the expense of shear flow energy, with the help of the convective mode. We also quantified the efficiency of wave generation at different azimuthal and vertical wavenumbers and found that it is maximal when these length-scales are comparable to the disc scale height. This, in turn, implies that SDWs excited by convection have weak vertical dependence, similar to SDWs generated by vortices (see HP09a). We calculated the angular momentum flux associated with non-axisymmetric SDWs generated by the convective mode and found that it is positive, i.e., transport is outward as opposed to that of the convective mode.

Studied here linear coupling of SDWs and convection is basically similar in nature to the linear coupling of SDWs and vortices that has already been extensively studied (Bodo et al. 2005; Mamatsashvili & Chagelishvili 2007, HP09a) and represents a special manifestation of a more general phenomenon of shear-induced linear coupling of perturbation modes inevitably taking place in any flow with an inhomogeneous velocity profile, or shear. Thus, although convection is not generally shear-driven – in that it does not directly tap energy from shear but from the unstable superadiabatic thermal distribution – its dynamics is still affected by shear and shear-induced coupling to SDWs, in some sense, makes convection a participant in kinematic processes as well.

Shearing box simulation of compressible MRI-turbulence in a Keplerian disc indicates that the angular momentum transport due to non-axisymmetric SDWs generated by vortical perturbations constitutes a significant fraction of that associated with the total turbulent Reynolds stresses (Heinemann & Papaloizou 2009b). In other words, a purely hydrodynamic part of transport is mostly due to these SDWs and is quite appreciable. As mentioned in the Introduction, in their non-linear simulations, Lesur & Ogilvie (2010) demonstrated that, contrary to previous results, in fact vertical convection in

⁴ But overall, wave perturbations and associated transport are not damped in a fully developed turbulence, as successive leading SFHs are regenerated due to non-linearity, maintaining a steady angular momentum flux.

protoplanetary discs has a non-axisymmetric structure and is thus able to transport angular momentum outwards. But the magnitude of the corresponding α reported in their simulations is still small ($\lesssim 10^{-4}$). However, these simulations were performed in the Boussinesq/incompressible limit, where high-frequency SDWs are filtered out. In a related study, Käpylä et al. (2010) solved full hydrodynamical equations in the shearing box with superadiabatic stratification without explicitly making the assumption of incompressibility, but the parameter regime considered was such as to give small Mach numbers. So, the effects of compressibility and, hence of SDWs, were probably small in their simulations and were not particularly addressed. As noted above, SDWs are generally known to be able to enhance angular momentum transport rates. For example, Johnson & Gammie (2005b) demonstrated that compressible simulations of vortices in 2D discs yield at least an order of magnitude larger transport rate, which is primarily due to shocks of SDWs emitted by vortices, compared with that in the incompressible case, which is due to vortices only. Based on this property, we might anticipate a similar situation if compressibility is taken into account in simulations of convectively unstable discs, where SDWs generated by convective motions in the non-linear regime could also boost outward angular momentum transport due to convection alone, although this needs to be further investigated in greater detail in future numerical studies. We emphasise once more that the described here shear-induced coupling between the SDWs and convection occurs only when these modes are non-axisymmetric. So, in the earlier simulations of Cabot (1996) and Stone & Balbus (1996), where vertical convection had an axisymmetric structure, SDW generation could not be observed in spite of moderate Mach numbers associated with convective motions. Another point, which also merits investigation is where in the disc SDWs generated by convection primarily cause dissipation through shock formation (see also Stone & Balbus 1996), because in all the above-mentioned simulations convection was not generated self-consistently, but maintained by an artificially imposed heat flux. This becomes even more interesting in the light of the result obtained here that in the linear regime SDWs do not vary much with height. If the shocks of SDWs dissipate near the surface, this may stifle convection via reducing the negative entropy gradient, while if – near the midplane, this can then sustain convection.

Finally, we would like to mention that strong vertical convection also occurs in FU Orionis systems during outbursts as a result of hydrogen ionisation and is one of the important factors for understanding the nature of the outburst phenomenon (Zhu et al. 2009). In this case, as shown by Zhu et al., convection is confined to the inner disc, extends over the whole vertical height and causes strong density fluctuations, because the Mach number of the convective eddies/motions is of the order of unity. In other words, convection is compressible, so the question of the SDW excitation and the role of wave transport in the outburst process seems relevant for further investigation.

ACKNOWLEDGMENTS

G.R.M. would like to acknowledge the financial support from the Scottish Universities Physics Alliance (SUPA). He thanks G. D. Chagelishvili and A. G. Tevzadze for critically reading the manuscript. The useful and constructive comments from the anonymous referee, that improved the presentation of our work, are also much appreciated.

REFERENCES

- Armitage P. J., Livio M., Pringle J. E., 2001, *MNRAS*, 324, 705
- Balbus S. A., 2003, *ARA & A*, 41, 555
- Balbus S. A., Hawley J. F., 1992, *ApJ*, 400, 610
- Balbus S. A., Hawley J. F., 1998, *Rev. Mod. Phys.*, 70, 1
- Blaes O. M., Balbus S. A., 1994, *ApJ*, 421, 163
- Bodo G., Chagelishvili G., Murante G., Tevzadze A., Rossi P., Ferrari A., 2005, *A&A*, 437, 9
- Bodo G., Tevzadze A., Chagelishvili G., Mignone A., Rossi P., Ferrari A., 2007, *A&A*, 475, 51
- Brandenburg A., Dintrans B., 2006, *A&A*, 450, 437
- Cabot W., 1996, *ApJ*, 465, 874
- Cabot W., Pollack J. B., 1992, *Geophys. Astrophys. Fluid Dyn.*, 64, 97
- Cameron A. G. W., 1978, *Moon and Planets*, 18, 5
- Chagelishvili G. D., Rogava A. D., Tsiklauri D. G., 1996, *Phys. Rev. E*, 53, 6028
- Chagelishvili G. D., Tevzadze A. G., Bodo G., Moiseev S. S., 1997, *Phys. Rev. Lett.*, 79, 3178
- Davis S. S., 2002, *ApJ*, 576, 450
- Davis S. S., Sheehan D. P., Cuzzi J. N., 2000, *ApJ*, 545, 494
- Desch S. J., 2004, *ApJ*, 608, 509
- Drazin P. G., Reid W. H., 1981, *Hydrodynamic Stability*. Cambridge University Press, Cambridge, UK
- Fleming T., Stone J. M., 2003, *ApJ*, 585, 908
- Fromang S., Terquem C., Balbus S. A., 2002, *MNRAS*, 329, 18
- Gammie C. F., 1996, *ApJ*, 457, 355
- Goldreich P., Lynden-Bell D., 1965, *MNRAS*, 130, 125
- Hawley J. F., Gammie C. F., Balbus S. A., 1995, *ApJ*, 440, 742
- Heinemann T., Papaloizou J. C. B., 2009a, *MNRAS*, 397, 52
- Heinemann T., Papaloizou J. C. B., 2009b, *MNRAS*, 397, 64
- Johnson B. M., Gammie C. F., 2005a, *ApJ*, 626, 978
- Johnson B. M., Gammie C. F., 2005b, *ApJ*, 635, 149
- Johnson B. M., Gammie C. F., 2006, *ApJ*, 636, 63
- Käpylä P. J., Brandenburg A., Korpi M. J., Snellman J. E., Narayan R., 2010, *ApJ*, 719, 67
- Klahr H. H., Bodenheimer P., 2003, *ApJ*, 582, 869
- Klahr H. H., Henning T., Kley W., 1999, *ApJ*, 514, 325
- Kley W., Papaloizou J. C. B., Lin D. N. C., 1993, *ApJ*, 416, 679
- Korycansky D. G., 1992, *ApJ*, 399, 176
- Korycansky D. G., Pringle J. E., 1995, *MNRAS*, 272, 618
- Latter H. N., Balbus S. A., 2009, *MNRAS*, 399, 1058
- Lerche I., Parker E. N., 1967, *ApJ*, 149, 559
- Lesur G., Ogilvie G. I., 2010, *MNRAS*, 404, L64

- Lesur G., Papaloizou J. C. B., 2010, *A&A*, 513, 60
- Li H., Colgate S. A., Wendroff B., Liska R., 2001, *ApJ*, 551, 874
- Li L., Goodman J., Narayan R., 2003, *ApJ*, 593, 980
- Lin D. N. C., Papaloizou J., 1980, *MNRAS*, 191, 37
- Lin D. N. C., Papaloizou J., 1985, in D. C. Black & M. S. Matthews ed., *Protostars and Planets II*, On the dynamical origin of the solar system. Tucson, AZ, University of Arizona Press, pp 981–1072
- Lin D. N. C., Papaloizou J. C. B., Kley W., 1993, *ApJ*, 416, 689
- Lin D. N. C., Papaloizou J. C. B., Savonije G. J., 1990, *ApJ*, 364, 326
- Lovelace R. V. E., Li H., Colgate S. A., Nelson A. F., 1999, *ApJ*, 513, 805
- Lubow S. H., Ogilvie G. I., 1998, *ApJ*, 504, 983
- Lubow S. H., Pringle J. E., 1993, *ApJ*, 409, 360
- Mamatsashvili G. R., Chagelishvili G. D., 2007, *MNRAS*, 381, 809
- Mamatsashvili G. R., Rice W. K. M., 2009, *MNRAS*, 394, 2153
- Mamatsashvili G. R., Rice W. K. M., 2010, *MNRAS*, 406, 2050
- Narayan R., Goldreich P., Goodman J., 1987, *MNRAS*, 228, 1
- Nelson R. P., 2005, *A&A*, 443, 1067
- Nelson R. P., Papaloizou J. C. B., 2004, *MNRAS*, 350, 849
- Ogilvie G. I., 1998, *MNRAS*, 297, 291
- Ogilvie G. I., Lubow S. H., 1999, *ApJ*, 515, 767
- Oishi J. S., Mac Low M., 2009, *ApJ*, 704, 1239
- Oishi J. S., Mac Low M., Menou K., 2007, *ApJ*, 670, 805
- Petersen M. R., Stewart G. R., Julien K., 2007, *ApJ*, 658, 1252
- Rafikov R. R., 2007, *ApJ*, 662, 642
- Ruden S. P., Lin D. N. C., 1986, *ApJ*, 308, 883
- Ruden S. P., Papaloizou J. C. B., Lin D. N. C., 1988, *ApJ*, 329, 739
- Ruden S. P., Pollack J. B., 1991, *ApJ*, 375, 740
- Rüdiger G., Tschäpe R., Kitchatinov L. L., 2002, *MNRAS*, 332, 435
- Ryu D., Goodman J., 1992, *ApJ*, 388, 438
- Salmeron R., Wardle M., 2003, *MNRAS*, 345, 992
- Sano T., Miyama S. M., Umebayashi T., Nakano T., 2000, *ApJ*, 543, 486
- Sano T., Stone J. M., 2002, *ApJ*, 577, 534
- Schmid P. J., Henningson D. S., 2001, *Stability and Transition in Shear Flows*. Springer Verlag
- Shu F. H., 1974, *A&A*, 33, 55
- Stone J. M., Balbus S. A., 1996, *ApJ*, 464, 364
- Stone J. M., Gammie C. F., Balbus S. A., Hawley J. F., 2000, in V. Mannings A. P. Boss S. S. R., ed., *Protostars and Planets IV*, Transport processes in protostellar disks. Tucson: University of Arizona Press, p. 589
- Tevezadze A. G., Chagelishvili G. D., Bodo G., Rossi P., 2010, *MNRAS*, 401, 901
- Tevezadze A. G., Chagelishvili G. D., Zahn J., 2008, *A&A*, 478, 9
- Tevezadze A. G., Chagelishvili G. D., Zahn J., Chanishvili R. G., Lominadze J. G., 2003, *A&A*, 407, 779
- Thompson W., 1887, *Philos. Mag*, 24, 188
- Trefethen L. N., Trefethen A. E., Reddy S. C., Driscoll T. A., 1993, *Science*, 261, 578
- Turner N. J., Sano T., Dziourkevitch N., 2007, *ApJ*, 659, 729
- Yoshida Z., 2005, *Phys. Plasmas*, 12, 024503
- Zhu Z., Hartmann L., Gammie C., McKinney J. C., 2009, *ApJ*, 701, 620